Inorganic Chemistry

Article

pubs.acs.org/IC

Dinuclear Ru/Ni, Ir/Ni, and Ir/Pt Complexes with Bridging Phenanthroline-5,6-dithiolate: Synthesis, Structure, and Electrochemical and Photophysical Behavior

David Schallenberg,[†] Antje Neubauer,*[,‡] Elisa Erdmann,[†] Marco Tänzler,[†] Alexander Villinger,[†] Stefan Lochbrunner,[‡] and Wolfram W. Seidel*[,†]

[†]Institut für Chemie, Universität Rostock, Albert-Einstein-Straße 3a, 18059 Rostock, Germany

[‡]Institut für Physik, Universität Rostock, Universitätsplatz 3, 18051 Rostock, Germany

Supporting Information

ABSTRACT: We report the synthesis and full characterization of dinuclear complexes with the bridging ligand phenanthroline-5,6-dithiolate (phendt^{2-}) featuring the $[Ru(bpy)_2]^{2+}$ or $Ir(ppy)_2]^{+}$ fragment at the diimine donor center and the $[Ni(dppe)]^{2+}$ or $[Pt(phen)]^{2+}$ complex moiety at the dithiolate group. The molecular structures of the mononuclear complexes $[(C_5H_5)_2Ti(S,S'\text{-phendt})]$ and $[(ppy)_2Ir\{N,N'\text{-phendt-}(C_2H_4CN)_2\}](PF_6)$ as well as the dinuclear complex $[(C_5H_5)(PPh_3)Ru(phendt)Ni(dppe)](PF_6)$ determined by X-ray diffraction (XRD) studies are compared. Photophysical studies with mononuclear $[(bpy)_2Ru\{phendt\text{-}(C_2H_4CN)_2\}]^{2+}$ and $[(ppy)_2Ir\{phendt\text{-}(C_2H_4CN)_2\}]^{+}$ as well as dinuclear $[(bpy)_2Ru(phendt)Ni(dppe)]^{2+}$ and $[(ppy)_2Ir(phendt)Ni(dppe)]^{+}$ uncovered an effective luminescence quenching in the dinuclear complexes. Lifetime measurements at room temperature, steady-state measurements at low temperature, electrochemical investigations, and DFT calculations provide evidence for a very efficient energy transfer from the Ru/Ir to the Ni complex moiety with a rate constant $k > 5 \times 10^9$ s^{-1}. In comparison, the [Ru]phendt[Ni] complex displays a higher quenching efficiency with reduced excited state lifetime, whereas the [Ir]phendt[Ni] complex is characterized by an unaltered lifetime of the thermally equilibrated excited state.

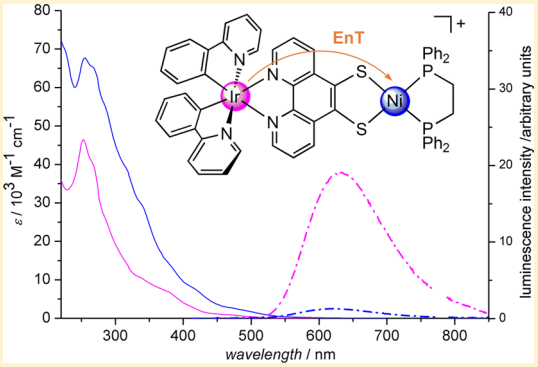

INTRODUCTION

Sun-powered photocatalytic processes can contribute in the future to an environmentally friendly supply of fuel or valuable substances. Charge and energy transfer are the key elements in photocatalysis, and their understanding and optimization are of crucial importance. In nature, light-driven charge separation is based on a firm spatial alignment of redox centers on the electron path. Biomimetic artificial systems typically rely on straightforwardly constructed unsaturated ligand systems bearing alkyne, phenylene, or vinylene building blocks. On this basis, a variety of polynuclear complexes with Ru(II) or Ir(III) chromophores utilizing specifically designed poly(pyridine) ligands have shown remarkable potential for charge separation or energy transfer.[1,2] Potential applications in electroluminescence,[3,4] photocatalysis,[5,6] dye-sensitized solar cells,[2,7] luminescent biosensors,[8] and triplet−triplet annihilation upconversion[9] have caused a tremendous research activity in the field. Phenanthrolines (phen) with donor substituents in the 5,6-position are particularly rigid, complying a beneficial condition for very fast electron transfer processes between metals linked by those ligands. Accordingly, extended phenanthroline type ligands like tetrapyridophenazines or pyridinoxazol phenanthrolines connecting a $Ru^{II}(diimine)_2$ photosensitizer with catalytic Pd, Rh, or cobaloxime centers have shown remarkable photocatalytic dihydrogen production.[5,10]

Bridging two metal centers by phenanthroline-5,6-diolate has been thoroughly investigated by Pierpont and Eisenberg proving the strong intermetallic electronic cooperativity in those systems.[11,12] With respect to light-driven charge separation, such ligands with different coordination sites are particularly interesting, because they are directional. The sulfur congener phenanthroline-5,6-dithiolate, phendt^{2-}, $\mathbf{1}^{2-}$, is intriguing because of its potential use in biomimetic hydrogenase models and nonlinear optical materials. Phenanthroline derivatives with sulfur substitution in the 5,6-position and respective monomolecular complexes with Ru(II) have been reported by Almeida,[13] Hudhomme,[14] and Shatruk,[15,16] but these studies were focused on the electronic fine-tuning and the donor ability of the ligand, whereas the option for 1,2-dithiolate coordination was not utilized. Due to the relative separation of the C=C double bond in the 5,6-position from the aromatic pyridine systems in phenanthrolines, the corresponding 5,6-dithiolate should rather behave like a classical dithiolene donor. Generally, dithiolene complexes show strong absorptions in the

Received: December 20, 2013
Published: August 20, 2014

   dx.doi.org/10.1021/ic4031206 | Inorg. Chem. 2014, 53, 8859−8873

visible range[17] and redox variability at moderate potentials;[18] hence, linking them covalently to photosensitizers is an attractive goal. Accordingly, polynuclear complexes with the bridging ligand $\mathbf{1}^{2-}$ have been suggested by Eisenberg[12] as desirable building blocks for light energy conversion materials, but characterized examples are not published until now. In this contribution, we present such dinuclear complexes with $\mathbf{1}^{2-}$, and we discuss our investigations on their electrochemical and photophysical behavior focusing on the function of the novel bridging ligand.

EXPERIMENTAL SECTION

Characterization of Compounds. One- and two-dimensional NMR spectra were recorded at 300 K with a BrukerAvance 250, 300, or 500 MHz spectrometer, respectively. In ^{1}H and ^{13}C NMR, the chemical shifts were internally referenced to the solvent residual peak (^{1}H NMR: 7.26 ppm in $CDCl_3$ and 1.94 ppm in CD_3CN; ^{13}C NMR: 77.2 ppm in $CDCl_3$ and 118.3 ppm in CD_3CN), and in ^{31}P NMR, H_3PO_4 was used as external standard. IR spectroscopy was conducted on a Nicolet 380 FT-IR with a Smart Orbit ATR module. Elemental analyses were performed with a Thermo Finnigan Flash EA 1112 Series, determination of sulfur being excluded for compounds with fluorine content. Mass spectrometry by Electrospray Ionization (ESI) was obtained with an Agilent 6210 Time-of-Flight LC/MS or with a Thermo Electron Finnigan MAT 95-XP spectrometer. Cyclic voltammetry was performed using a Princeton Applied Research VersaSTAT 3. A three electrode arrangement with a glassy carbon working electrode, a platinum wire counter electrode and a Ag/AgCl in CH_3CN reference electrode and 0.15 M n-Bu_4NPF_6 as supporting electrolyte was employed. The ferrocene/ferrocenium (Fc/Fc^+) redox couple was used as internal standard.

X-ray Crystallography. Single crystals suitable for X-ray diffraction analysis were selected in Fomblin YR-1800 perfluoropolyether oil (Alfa Aesar) at ambient temperature and mounted on a glass fiber. During the measurement, the samples were cooled to 173(2) K. Diffraction data were collected on a Bruker-Nonius Apex X8 and a Bruker Kappa Apex II diffractometer using graphite monochromated Mo Kα radiation. Structure solutions were found by direct methods (SHELXS-97) and were refined by full-matrix least-squares procedures on F^2 (SHELXL-97). All non-hydrogen atoms were refined anisotropically, and hydrogen atoms were included at calculated positions with fixed thermal parameters.

Absorption and Luminescence Measurements. Steady-state UV−vis absorption spectra were recorded with a PerkinElmer Lambda 19 or an Analytik Jena Specord 50 spectrophotometer and steady-state emission spectra with a Fluoromax-4 spectrofluorometer (Horiba Scientific). The solvents CH_3CN, CH_2Cl_2, and $CHCl_3$ were of Uvasol-quality (Merck). The samples were placed in a 1 cm path fused silica cuvette, and dissolved oxygen was removed by bubbling with argon for about 5 min. Corrected emission spectra were obtained via a calibration curve supplied with the instrument. Photoluminescence quantum yields (φ_{PL}) were extracted from corrected spectra on a wavelength scale (nm). A solution of $[Ru(bpy)_3]Cl_2$ (Tris(2,2′-bipyridine)dichlororuthenium(II)-hexahydrate, Aldrich) in air-equilibrated water (spectrophotometric grade, Alfa Aesar) was applied as standard (φ_{PL} = 0.028).[19] The different refractive indices for luminescence standard and sample solvent were corrected for.[20] Sample and luminescence standard were excited at 388 nm with an absorbance of about 0.1 at the excitation wavelength for both sample and standard. Photoluminescence lifetimes (τ_{PL}) were determined with a Hamamatsu Photonics Streak-camera system operating in a single photon counting mode and providing a time-resolution of about 200 ps. The samples were optically excited at λ_{exc} = 388 nm by a fraction of the output of a 1 kHz regenerative Ti:sapphire amplifier system (CPA 2001; Clark MXR), which was frequency-doubled. The excitation intensity was ranging from 1×10^{11} to 3×10^{12} photons cm^{-2} per pulse. Analysis of the photoluminescence decay curves versus time was performed with the Analysis Software (TAFit32; version 1.12) provided by Hamamatsu Photonics. The quality of the fit was assessed by the χ^2 value. Cryogenic steady-state emission spectra were recorded with an Agilent Cary Eclipse spectrometer and with the help of a Variable Temperature Cell Holder (Specac). The solvent C_3H_7CN was purchased from Alfa Aesar and dissolved oxygen was removed by bubbling with argon for about 2 h. Liquid nitrogen was used as refrigerant.

DFT Calculations. The calculations were performed with the Gaussian 09 program package. The electronic structure was further analyzed using the AOMix program.[21] The computations were carried out as closed shell calculations for the complex cations $[(ppy)_2Ir(phendtH_2)]^+$ $\mathbf{5a}^{2+}$ and $[(ppy)_2Ir(phendtH_2)]^+$, $\mathbf{6a}^+$ (modeling complexes $\mathbf{5}^{2+}$ and $\mathbf{6}^+$), as well as for $\mathbf{8}^{2+}$ and $\mathbf{10}^+$. The hybrid functionals used were varied from b3lyp[22] to CAM-b3lyp[23] and lc-blyp.[24] Ir(Ru) was described by pseudorelativistic effective core potentials (ECP) of the Stuttgart/Cologne group for 60(28) core electrons and (8s7p6d2f1g)/[6s5p3d2f1g] basis sets.[25] A 6-311G(d,p) basis set was used for the remaining elements C, H, N, Ni, P, and S. Molecular geometries were optimized for imposed C_2 symmetry in the gas phase as well as using a polarizable solvent continuum model (PCM). TD-DFT calculations were conducted for 20 singlet singlet and 6 singlet triplet transitions. Further details are given in the Supporting Information.

Materials and Synthesis. All operations were carried out in an atmosphere of dry argon using Schlenk and glovebox techniques. Solvents were dried and saturated with argon by standard methods and freshly distilled prior to use. Dry DMF was obtained by Sigma-Aldrich. Bn_2-**1**,[15] 3-mercaptopropionitrile,[26] 5,6-dibromo-1,10-phenanthroline,[15] $[(C_5H_5)(PPh_3)Ru(NCMe)_2]PF_6$,[27] $[(bipy)_2RuCl_2]\cdot 2H_2O$,[28] $[(ppy)_2IrCl]_2$,[29] $[Ni(dppe)Cl_2]$, $[Ni(dppv)Cl_2]$,[30] and $[Pt(phen)Cl_2]$[31] were prepared according to literature methods. All other chemicals (at least of reaction grade quality) were obtained from commercial sources and used as received. Analytical thin layer chromatography was performed on silica gel (Silica 60 F254) or on aluminum oxide (aluminum oxide 150 F254) coated aluminum plates. Column chromatography was performed using silica gel 60 (pore size 0.063−0.2 mm) or aluminum oxide 90 (neutral, pore size 0.063−0.2 mm) purchased from Merck as the column stationary phase.

Synthesis of $[(C_5H_5)_2Ti(S,S'\text{-}1)]$ (2). A suspension of Bn_2-**1** (401 mg, 0.94 mmol) and dry $AlCl_3$ (1.01 g, 7.58 mmol) in toluene (40 mL) was stirred at ambient temperature overnight. The volume was reduced by the half in vacuo and decanted. The slurry residue was hydrolyzed with degassed water (30 mL) at 0 °C followed by the addition of a degassed 2 M NaOH solution (35 mL) and filtration. Careful neutralization with diluted aqueous HCl to adjust pH 3−4 gave a brown precipitate, which was isolated by filtration, washed with water and diethyl ether, and dried in vacuo to afford crude H_2-

dx.doi.org/10.1021/ic4031206 | Inorg. Chem. 2014, 53, 8859−8873

1. The crude H_2-**1** and $[(C_5H_5)_2TiCl_2]$ (210 mg, 0.84 mmol) were suspended in THF (40 mL). After addition of NEt_3 (288 μL, 210 mg, 2.08 mmol), the mixture was stirred overnight at ambient temperature. Subsequently, the solvent was removed in vacuo. The residue was purified by column chromatography on silica (CH_2Cl_2/MeOH/aqueous NH_3 25%, 20:1:0.5) to afford a dark green solid. Yield: 9% (25 mg, 0.08 mmol). Alternatively, a mixture of **3** (700 mg, 2 mmol) and potassium-*tert*-butanolate (*tert*-BuOK) (500 mg, 4.46 mmol) was dissolved in DMF (15 mL), and the resulting dark red solution was stirred for 2 h at ambient temperature. Subsequently, solid $[(C_5H_5)_2TiCl_2]$ (450 mg, 1.81 mmol) was added, and the reaction mixture was stirred for an additional hour. The solvent and the byproducts *tert*-BuOH and acrylonitrile were removed in vacuo. Finally, the residue was purified as described above. Recrystallization from CH_2Cl_2/*n*-pentane gave pure **2**. Yield: 56% (450 mg, 1.01 mmol). Single crystals of **2** suitable for XRD analysis were obtained by vapor diffusion of *n*-pentane into a solution of **2** in fluorobenzene. Anal. Calcd for $C_{22}H_{16}S_2Ti$: C, 62.86; H, 3.84; N, 6.66. Found: C, 62.67; H, 3.81; N, 6.75. ^{1}H NMR ($CDCl_3$, 300 MHz), δ/ppm: 9.18 (*m*, 2H, 2/9-phen-*H*), 8.08 (dd, J = 8.3 Hz, J = 1.7 Hz, 2H, 4/7-phen-*H*), 7.63 (dd, J = 8.3 Hz, J = 1.7 Hz, 2H, 3/8-phen-*H*), 6.03 (br, 10H, C_5H_5). ^{13}C NMR ($CDCl_3$, 75.5 MHz), δ/ppm: 153.1 (5/6-phen-*C*), 149.1 (2/9-phen-*C*), 145.2 (12/14-phen-*C*), 135.8 (4/7-phen-*C*), 129.5 (13/14-phen-*C*), 123.2 (3/8-phen-*C*), 111.6 (C_5H_5). ESI + (MeOH/0.1% HCOOH in H_2O 90:10), m/z (M = $[(C_5H_5)_2Ti(S,S'$-**1**$)]$, relative intensity): 421 ($[M + H^+]$, 100). UV−vis (CH_3CN), λ/nm (ε/M^{-1} cm^{-1}): 222 (41 200), 226 (41 000), 236 (35 300), 268 (33 600), 305 (12 600), 345 (6000), 456 (2000), 631 (1800).

Synthesis of (NC-C_2H_4)$_2$-1 (3). A solution containing 3-mercaptopropionitrile (1.35 g, 15.5 mmol) in DMF (25 mL) was added to solid $NaOCH_3$ (846 mg, 15.7 mmol) at 0 °C and stirred for 15 min. The resulting solution was added to 5,6-dibromo-1,10-phenanthroline (2.5 g, 7.4 mmol) at 0 °C, and the dark brown solution was stirred at ambient temperature overnight. The solvent was removed in vacuo, and the residue was extracted into CH_2Cl_2 (250 mL). The suspension was filtered and the solvent was removed in vacuo to give a brown solid residue, which was purified by column chromatography on silica (CH_2Cl_2/MeOH/aqueous NH_3 25%, 20:1:0.5, R_f = 0.87) to afford a beige solid. Yield: 41% (1.06 g, 3.03 mmol). Anal. Calcd for $C_{18}H_{14}N_4S_2$: C, 61.69; H, 4.03; N, 15.99 ; S, 18.30. Found: C, 62.08; H, 4.05; N, 15.93; S, 18.45. ^{1}H NMR ($CDCl_3$, 250 MHz), δ/ppm: 9.20 (m, 4H, 2/9- and 4/7-phen-*H*), 7.88 (dd, J = 8.4 Hz, J = 4.3 Hz, 2H, 3/8-phen-*H*), 3.28 (*t*, J = 6.9 Hz, 4H, SCH_2), 2.58 (t, J = 6.9 Hz, 4H, CH_2CN). ^{13}C NMR ($CDCl_3$, 62.9 MHz), δ/ppm: 150.9 (2/9-phen-*C*), 146.0 (5/6-phen-*C*), 138.0 (12/14-phen-*C*), 135.5 (4/7-phen-*C*), 129.6 (11/13-phen-*C*), 123.5 (3/8-phen-*C*), 117.5 (CH_2CN), 32.6 (SCH_2), 18.0 (CH_2CN). ESI+ (MeOH/0.1% HCOOH in H_2O 90:10), m/z (M = (NC-C_2H_4)$_2$- **1**, relative intensity): 373 ($[M + Na^+]$, 30), 351 ($[M + H^+]$, 100). IR (ATR), ν/cm^{-1}: 2244 (C≡N). UV/vis (CH_3CN), λ/nm (ε/M^{-1} cm^{-1}): 200 (21 300), 236 (36 100), 267 (17 000).

Synthesis of [(C_5H_5)Ru(PPh_3)(*N*,*N*′-3)](PF_6) (4-PF_6). CH_2Cl_2 (20 mL) was added to a mixture of **3** (135 mg, 0.39 mmol) and $[C_5H_5)(PPh_3)Ru(NCMe)_2]PF_6$ (250 mg, 0.38 mmol). The color of the resulting solution turned red immediately. After stirring for an hour at ambient temperature, the solvent was removed in vacuo. The residue was dissolved in CH_2Cl_2, filtered, and layered with a double amount of *n*-pentane to afford red, air-stable **4**-PF_6. Single crystals of **4**-PF_6 suitable for XRD analysis were obtained by vapor diffusion of *n*-pentane into a solution of **4**-PF_6 in $CHCl_3$.

Yield: 87% (301 mg, 0.33 mmol). Anal. Calcd for $C_{41}H_{34}F_6N_4P_2RuS_2{\cdot}CHCl_3$: C, 50.68; H, 3.54; N, 5.70. Found: C, 50.73; H, 3.52; N, 5.63. ^{1}H NMR (CD_3CN, 250 MHz), δ/ppm: 9.61 (d, J = 5.4 Hz, 2H, 2/9-phen-*H*), 8.95 (d, J = 8.5 Hz, 2H, 4/7-phen-*H*), 7.68 (dd, J = 8.5 Hz, J = 5.4 Hz, 2H, 3/8-phen-*H*), 7.25 (dd, J = 7.3 Hz, J = 1.6 Hz, 3H, *p*-Ph-*H*), 7.14 (m, 6H, *o*-Ph-*H*), 6.91 (m, 6H, *m*-Ph-*H*), 4.84 (*s*, 5H, C_5H_5), 3.23 (td, J = 6.7 Hz, J = 3.1 Hz, 4H, SCH_2), 2.67 (t, J = 7.5 Hz, 4H, CH_2CN). ^{13}C NMR (CD_3CN, 62.9 MHz), δ/ppm: 158.1 (2/9-phen-*C*), 148.7 (12/14-phen-*C*), 141.0 (5/6-phen-*C*), 136.1 (4/7-phen-*C*), 133.7 (*m*-Ph-*C*), 133.6 (*m*-Ph-*C*), 132.9 (*i*-Ph-*C*), 132.4 (11/13-phen-*C*), 131.7 (*i*-Ph-*C*), 131.1 (*p*-Ph-*C*), 131.0 (*p*-Ph-*C*), 129.3 (*o*-Ph-*C*), 129.2 (*o*-Ph-*C*), 125.9 (3/8-phen-*C*), 119.7 (CH_2CN), 79.3 (C_5H_5), 34.2 (SCH_2), 19.4 (CH_2CN). ^{31}P NMR (CD_3CN, 101.3 MHz), δ/ppm: 51.1 (s, PPh_3). ESI+ (MeOH/0.1% HCOOH in H_2O 90:10), m/z (M = $[(C_5H_5)Ru(PPh_3)(N,N'$-**3**$)]^+$, relative intensity): 779 ($[M^+]$, 100). IR (ATR), ν/cm^{-1}: 2250 (C≡N). UV/vis (CH_3CN), λ/nm (ε/M^{-1} cm^{-1}): 206 (62 200), 226 (43 900), 268 (22 100), 334 (6300), 421 (5100).

Synthesis of [(bpy)$_2$Ru(*N*,*N*′-3)](PF_6)$_2$ (5-(PF_6)$_2$). A suspension of $[(bipy)_2RuCl_2]{\cdot}2H_2O$ (1.3 g, 2.5 mmol) and **2** (900 mg, 2.6 mmol) in ethanol (160 mL) was refluxed for 4 h accompanied by a color change to red. The mixture was filtered followed by the addition of a saturated aqueous KPF_6-solution. The orange precipitate was isolated by filtration, washed with ethanol and diethyl ether and dried in vacuo to afford an air- and water-stable orange powder. Yield: 74% (1.95 g, 1.85 mmol). Anal. Calcd for $C_{38}H_{30}F_{12}N_8P_2RuS_2$: C, 43.31; H, 2.87; N, 10.63. Found: C, 43.00; H, 2.89; N, 10.68. ^{1}H NMR (CD_3CN, 300 MHz), δ/ppm: 9.26 (dd, J = 10.4 Hz, J = 1.2 Hz, 2H, 4/7-phen-*H*), 8.53 (dd, J = 11.4 Hz, J = 8 Hz, 4H, Ar-*H*), 8.17 (td, J = 5.1 Hz, J = 1.1 Hz, 2H, 2/9-phen-*H*), 8.11 (m, 2H, Ar-*H*), 8.02 (m, 2H, Ar-*H*), 7.84 (m, 4H, Ar-*H*), 7.46 (m, 4H, Ar-*H*), 7.24 (m, 2H, Ar-*H*), 3.34 (t, J = 6.7 Hz, 4H, SCH_2), 2.66 (t, J = 6.7 Hz, 4H, CH_2CN). ^{13}C NMR (CD_3CN, 75.5 MHz), δ/ppm: 158.2, 158.0, 154.3, 153.2, 153.0, 149.5, 142.0, 139.0, 138.9, 137.8, 134.1, 128.7, 128.5, 127.7, 125.5, 125.3, 118.4 (CH_2CN), 34.0 (SCH_2), 19.5 (CH_2CN). ESI+ (CH_3CN), m/z (M = $[(bpy)_2Ru(N,N'$-**3**$)]^+$, relative intensity): 909 ($[M^{2+}$+ $PF_6^-]$, 55), 382 ($[M^{2+}]$, 100). IR (ATR), ν/cm^{-1}: 2251 (C≡N). UV/vis(CH_3CN), λ/nm (ε/M^{-1} cm^{-1}): 235 (40500), 271 (55300), 286 (71500), 340 (9700), 419 (15 000), 450 (18 500).

Synthesis of [(ppy)$_2$Ir(*N*,*N*′-3)](PF_6) (6-PF_6). A yellow suspension of **3** (599 mg, 1.71 mmol) and $[(ppy)_2IrCl]_2$ (835 mg, 0.78 mmol) was stirred in a mixture of CH_2Cl_2 (27 mL) and ethanol (12 mL) at ambient temperature. After a few minutes an orange solution arose and the solvents were removed in vacuo. The residue was dissolved in ethanol and filtered followed by the addition of a saturated aqueous KPF_6-solution. The yellow precipitate was isolated by filtration, washed with diethyl ether and dried in vacuo to afford an air- and water-stable yellow powder. Yield: 85% (1.32 g, 1.33 mmol). Single crystals of **6**-PF_6 suitable for XRD analysis were obtained by vapor diffusion of diethyl ether into a solution of **6**-PF_6 in CH_2Cl_2. Anal. Calcd for $C_{40}H_{30}F_6IrN_6PS_2$: C, 48.23; H, 3.04; N, 8.44. Found: C, 48.38; H, 3.03; N, 8.48. ^{1}H NMR (CD_3CN, 500 MHz), δ/ppm: 9.35 (dd, J = 8.6 Hz, J = 1.3 Hz, 2H, 4/7-phen-*H*), 8.36 (dd, J = 5 Hz, J = 1.3 Hz, 2H, 2/9-phen-

dx.doi.org/10.1021/ic4031206 | *Inorg. Chem.* 2014, 53, 8859−8873

Table 1. Crystallographic Details of Compounds 2, 6-PF_6, and 7-PF_6

compound	2	6-PF_6·CH_2Cl_2	7-PF_6·1.5 C_6H_5F
empirical formula	$C_{22}H_{16}N_2S_2Ti$	$C_{41}H_{32}Cl_2F_6IrN_6PS_2$	$C_{70}H_{57.5}F_{7.5}N_2NiP_4RuS_2$
FW (g mol^{-1})	420.39	1080.92	1416.96
cryst syst	orthorhombic	monoclinic	triclinic
space group	$Pna2_1$	$C2/c$	P-1
a (Å)	10.8381(5)	18.2827(12)	14.0988(4)
b (Å)	16.1616(8)	17.2083(11)	14.6087(4)
c(Å)	10.5484(5)	15.2584(10)	16.5442(5)
α (deg)	90.00	90.00	115.0290(10)
β (deg)	90.00	122.7530(10)	90.898(2)
γ (deg)	90.00	90.00	99.323(2)
V ($Å^3$)	1847.67(15)	4037.3(5)	3033.21(15)
Z	4	4	2
ρ (g cm^{-3})	1.511	1.778	1.551
μ (mm^{-1})	0.698	3.651	0.803
measured reflns	10 421	34 484	96 341
indep reflns	3683	7002	21 423
reflns with $I > 2\sigma(I)$	2645	5989	12 850
R_{int}	0.0568	0.0353	0.0504
$R1$ ($F[I > 2\sigma(I)]$)	0.0470	0.0385	0.0483
$wR2$ (F^2[all data])	0.0958	0.1064	0.1192
GOF	0.970	1.054	0.965
params	242	289	764
CCDC no.	974 770	974 771	974 772

H), 8.06 (d, *J* = 8.2 Hz, 2H, Ar-*H*), 7.90 (m, 2H, 3/8-phen-*H*), 7.81 (m, 4H, Ar-*H*), 7.40 (m, 2H, Ar-*H*), 7.07 (td, *J* = 7.6 Hz, *J* = 1.3 Hz, 2H, Ar-*H*), 6.91 (m, 4H, Ar-*H*), 6.38 (dd, *J* = 7.6 Hz, *J* = 0.7 Hz, 2H, Ar-*H*), 3.32 (t, *J* = 6.8 Hz, 4H, SCH_2), 2.65 (t, *J* = 6.8 Hz, 4H, CH_2CN). ^{13}C NMR (CD_3CN, 62.9 MHz), δ/ppm: 168.4 (*C*Ir), 153.0 (2/9-phen-*C*), 150.8, 150.6, 148.8 (12/14-phen-*C*), 145.3, 142.1 (5/6-phen-*C*), 139.6, 139.5 (4/7-phen-*C*), 134.4 (11/13-phen-*C*), 132.7, 131.4, 128.5 (3/8-phen-*C*), 126.0, 124.4, 123.8, 120.9, 119.7 (CH_2CN), 34.0 (SCH_2), 19.5 (CH_2CN). ESI+ (CH_3CN), m/z (M = [(ppy)$_2$Ir(*N*,*N*′-**3**)]$^+$, relative intensity): 851 ([M^+], 100). IR (ATR), ν/cm^{-1}: 2248 (C≡N). UV−vis (CH_3CN), λ/nm (ε/M^{-1} cm^{-1}): 253 (48 000), 269 (40 600).

Synthesis of 7-PF_6. A mixture of red **4**-PF_6 (230 mg, 0.25 mmol) and *tert*-BuOK (92 mg, 0.82 mmol) was dissolved in DMF (10 mL), and the resulting dark red solution was stirred for an hour at ambient temperature. Solid [Ni(dppe)Cl_2] (132 mg, 0.25 mmol) was added and the reaction mixture was stirred overnight. The solvent and the byproducts *tert*-BuOH and acrylonitrile were removed in vacuo. The residue was purified by column chromatography on silica (CH_2Cl_2/MeOH 20:1) to afford a red solid. Recrystallization from CH_2Cl_2/*n*-pentane led to the pure product. Yield: 64% (205 mg, 0.16 mmol). Single crystals of 7-PF_6 suitable for XRD analysis were obtained by vapor diffusion of *n*-hexane into a solution of 7-PF_6 in fluorobenzene. Anal. Calcd for $C_{61}H_{50}F_6N_2NiP_4RuS_2$: C, 57.65; H, 3.96; N, 2.20. Found: C, 57.55; H, 3.94; N, 2.21. ^1H NMR (CD_3CN, 500 MHz), δ/ppm: 9.16 (d, *J* = 5.2 Hz, 2H, Ar-*H*), 8.25 (d, *J* = 8.3 Hz, 2H, Ar-*H*), 7.88−7.78 (m, 6H, Ar-*H*), 7.60−7.46 (m, 8H, Ar-*H*), 7.39 (m, 2H, Ar-*H*), 7.23 (dd, *J* = 8.3 Hz, *J* = 5.2 Hz, 2H, Ar-*H*), 7.19 (m, 3H, Ar-*H*), 7.11 (m, 2H, Ar-*H*), 7.03 (td, *J* = 7.7 Hz, *J* = 1.9 Hz, 4H, Ar-*H*), 6.82 (t, *J* = 8.9 Hz, 4H, Ar-*H*), 4.68 (s, 5H, C_5H_5), 2.56 (d, *J* = 18 Hz, 4H, CH_2). ^{13}C NMR (CD_3CN, 125.8 MHz), δ/ppm: 164.8, 162.8, 153.7, 146.6, 145.8 (t, *J* = 8.8 Hz), 134.7 (t, *J* = 5 Hz), 134.5 (t, *J* = 5 Hz), 133.5 (d, *J* = 11.3 Hz), 132.7 (d, *J* = 8.8 Hz), 132.3, 132.0, 131.5, 131.4, 130.9, 130.7, 130.5, 130.3, 130.0 (t, *J* = 5 Hz), 129.0 (d, *J* = 10 Hz), 125.4 (d, *J* = 2.5 Hz), 124.3, 116.2, 116.0, 78.8, 27.9 (t, *J* = 22.6 Hz, CH_2). ^{31}P NMR (CD_3CN, 202.5 MHz), δ/ppm: 59.5 (*s*, dppe-*P*), 52.0 (*s*, *P*Ph_3). ESI+ (CH_3CN), m/z (M = 7^+, relative intensity): 1127 ([M^+], 100). UV−vis (CH_3CN), λ/nm (ε/M^{-1} cm^{-1}): 212 (87 600), 223 (82 200), 274 (45 600), 321 (29 100), 370 (19 000), 496 (5000) (Table 1).

General Synthesis of the Dinuclear Complexes 8-$(PF_6)_2$, 9-$(PF_6)_2$, 10-PF_6, and 11-PF_6. A mixture of **5**-$(PF_6)_2$ or **6**-PF_6 and *tert*-BuOK was dissolved in DMF (10 mL), and the resulting dark red solution was stirred for an hour at ambient temperature. Solid [M(L^3)Cl_2] was added, and the reaction mixture was stirred overnight. The solvent and the byproducts *tert*-BuOH and acrylonitrile were removed in vacuo. The residue was purified by column chromatography on aluminum oxide (CH_2Cl_2/MeOH 20:1) to afford a red solid. Recrystallization from CH_2Cl_2/diethyl ether led to microcrystals of the pure product **8**-$(PF_6)_2$. Reactants: **5**-$(PF_6)_2$ (300 mg, 0.28 mmol), *tert*-BuOK (85 mg, 0.76 mmol), [Ni(dppe)Cl_2] (150 mg, 0.28 mmol). Yield: 48% (190 mg, 0.14 mmol). Anal. Calcd for $C_{58}H_{46}F_{12}N_6NiP_4RuS_2$: C, 49.66; H, 3.31; N, 5.99. Found: C, 49.83; H, 3.27; N, 5.94. ^1H NMR (CD_3CN, 300 MHz), δ/ppm: 8.63 (dd, *J* = 8.4 Hz, *J* = 0.9 Hz, 2H, Ar-*H*), 8.48 (t, *J* = 8.8 Hz, 4H, Ar-*H*), 8.05 (td, *J* = 10 Hz, *J* = 2.5 Hz, 2H, Ar-*H*), 7.95 (td, *J* = 7.5 Hz, *J* = 2.5 Hz, 2H, Ar-*H*), 7.87 (m, 4H, Ar-*H*), 7.87 (m, 4H, Ar-*H*), 7.79 (m, 8H, Ar-*H*), 7.59 (d, *J* = 6 Hz, 4H, Ar-*H*), 7.52 (m, 8H, Ar-*H*), 7.41 (d, *J* = 6.3 Hz, 2H, Ar-*H*), 7.18 (d, *J* = 6.3 Hz, 2H, Ar-*H*), 2.60 (m, 4H, CH_2). ^{13}C NMR (CD_3CN, 63 MHz), δ/ppm: 158.3, 158.0, 152.9, 149.8, 147.1, 146.9, 146.7, 138.7, 138.5, 134.7 (t, *J* = 5 Hz), 134.5 (t, *J* = 5 Hz), 133.6, 132.9, 132.8, 131.9, 131.1, 130.7, 130.3, 130.1, 130.0, 128.5, 128.4, 126.4, 125.2, 125.1, 28.1 (t, *J* = 24 Hz, CH_2). ^{31}P NMR (CD_3CN, 121.5 MHz), δ/ppm: 60.0 (*s*, dppe-*P*). ESI+ (CH_3CN), m/z (M = 8^{2+}, relative intensity): 556 ([M^{2+}], 100). UV−vis (CH_3CN), λ/nm (ε/M^{-1} cm^{-1}):

dx.doi.org/10.1021/ic4031206 | Inorg. Chem. 2014, 53, 8859−8873

226 (76 300), 255 (54 600), 286 (81 000), 329 (25 500), 427 (15 800), 460 (13 500). **9**-$(PF_6)_2$. Reactants: **5**-$(PF_6)_2$ (262 mg, 0.25 mmol), *tert*-BuOK (64 mg, 0.57 mmol), $[Ni(dppv)Cl_2]$ (130 mg, 0.25 mmol). Yield: 52% (182 mg, 0.13 mmol). Anal. Calcd for $C_{58}H_{42}F_{12}N_6NiP_4RuS_2$: C, 49.73; H, 3.17; N, 6.00. Found: C, (49.57); H, (3.14); N, (6.07). ^{1}H NMR (CD_3CN, 300 MHz), δ/ppm: 8.75−8.37 (m, 6H, Ar-*H*), 8.24−8.03 (m, 5H, Ar-*H*), 7.94 (m, 2H, Ar-*H*), 7.87−7.74 (m, 9H, Ar-*H*), 7.66−7.34 (m, 18H, Ar-*H*), 7.28−7.14 (m, 2H, Ar-*H*), 7.05−6.65 (m, 2H, Ar-*H*), 2.05 (s, 2H, PC*H*). ^{13}C NMR (CD_3CN, 75.5 MHz), δ/ppm: 158.3, 158.1, 158.0, 157.9, 152.9, 150.0, 148.4, 148.0, 147.5, 146.8, 139.1, 138.9, 138.7, 138.5, 134.3 (t, J = 6 Hz), 133.6, 133.5, 133.0, 131.8, 130.9, 130.7, 130.6, 130.3 (t, J = 5 Hz), 128.5 (t, J = 8 Hz), 126.4, 125.4, 125.3, 125.2, 125.1, 30.1 (PCH). ^{31}P NMR (CD_3CN, 121.5 MHz), δ/ppm: 68.0 (*s*, dppv-*P*). ESI+ (CH_3CN), m/z (M = $\mathbf{9}^{2+}$, relative intensity): 555 ([M^{2+}], 100). UV−vis (CH_3CN), λ/nm (ε/M^{-1} cm^{-1}): 208 (77 500), 231 (59 000), 254 (44 400), 286 (74 500), 432 (17 700), 444 (17 600), 462 (15 600). **10**-PF_6. Reactants: **6**-PF_6 (150 mg, 0.15 mmol), *tert*-BuOK (38 mg, 0.34 mmol), $[Ni(dppe)Cl_2]$ (78 mg, 0.15 mmol). Yield: 53% (109 mg, 0.08 mmol). Anal. Calcd for $C_{60}H_{46}F_6IrN_4NiP_3S_2$: C, 53.58; H, 3.45; N, 4.17. Found: C, 53.09; H, 3.44; N, 4.19. ^{1}H NMR (CD_3CN, 250 MHz), δ/ppm: 8.68 (dd, J = 8.5 Hz, J = 1.4 Hz, 2H, Ar-*H*), 7.95 (m, 4H, Ar-*H*), 7.90−7.39 (m, 23H, Ar-*H*), 7.35 (dd, J = 5.9 Hz, J = 0.9 Hz, 3H, Ar-*H*), 6.98 (m, 3H, Ar-*H*), 6.86 (m, 3H, Ar-*H*), 6.73 (ddd, J = 7.4 Hz, J = 5.9 Hz, J = 1.3 Hz, 2H, Ar-*H*), 6.31 (dd, J = 7.4 Hz, J = 0.9 Hz, 2H, Ar-*H*), 2.59 (m, 4H, CH_2). ^{13}C NMR (CD_3CN, 62.9 MHz), δ/ppm: 168.5, 151.8, 150.3, 148.6, 146.9 (t, J = 10 Hz), 145.8, 145.2, 139.2, 135.1, 134.8 (t, J = 5 Hz), 134.5 (t, J = 5 Hz), 132.8, 132.7, 132.3, 131.1, 130.6, 130.2, 130.0, 127.0, 125.8, 124.3, 123.5, 120.6, 23.9 (CH_2). ^{31}P NMR (CD_3CN, 121.5 MHz), δ/ppm: 60.0 (*s*, dppe-*P*). ESI+ (CH_3CN), m/z (M = $\mathbf{10}^+$, relative intensity): 1199 ([M^+], 100). UV−vis (CH_3CN), λ/nm (ε/M^{-1} cm^{-1}): 256 (70 700), 272 (66 600).

11-PF_6. Reactants: **6**-PF_6 (150 mg, 0.15 mmol), *tert*-BuOK (37 mg, 0.34 mmol), $[Pt(phen)Cl_2]$ (68 mg, 0.15 mmol). Yield: 60% (113 mg, 0.09 mmol). Anal. Calcd for $C_{46}H_{30}F_6IrN_6PPtS_2$: C, 43.74; H, 2.39; N, 6.65. Found: C, 43.64; H, 2.38; N, 6.57. ^{1}H NMR (CD_3CN, 300 MHz), δ/ppm: 8.78 (m, 2H, Ar-*H*), 8.27 (m, 2H, Ar-*H*), 8.09 (m, 4H, Ar-*H*), 7.78 (m, 6H, Ar-*H*), 7.67 (m, 2H, Ar-*H*), 7.57 (m, 2H, Ar-*H*), 7.19−6.96 (m, 6H, Ar-*H*), 6.88 (m, 2H, Ar-*H*), 6.55 (m, 2H, Ar-*H*), 6.43 (m, 2H, Ar-*H*). ESI+ (CH_3CN), m/z (M = $\mathbf{11}^+$, relative intensity): 1118 ([M^+], 100). UV−vis (CH_3CN), λ/nm (ε/M^{-1} cm^{-1}): 196 (76 300), 226 (61 400), 262 (61 100), 317 (22 800), 371 (12 400), 449 (5700), 532 (2200).

RESULTS

Synthesis. Our initial investigations revealed difficulties in isolating phenanthroline-5,6-dithiol probably due to a zwitterionic species at acid base equilibrium in solution (Scheme 1). After removal of benzyl groups in Bn_2-**1** with $AlCl_3$ in toluene according to a protocol of Shatruk et al.[15] we could isolate crude H_2-**1** in low yields. Reaction of H_2-**1** with $[(C_5H_5)_2TiCl_2]$ in the presence of NEt_3 delivered the titanocene complex $[(C_5H_5)_2Ti(S,S'$-**1**$)]$, **2**, with free nitrogen donor sites. Titanocene was chosen due to its halophilicity, which was thought to allow a *trans*-metalation with thiophilic metal centers like group 10 halogenides after coordination of a second metal ion at the diimine moiety. The identity of **2** was proven by full standard characterization (NMR, mass-spectrometry)

Scheme 1. Synthesis of the Phendt^{2-}dithiolato Complex 2

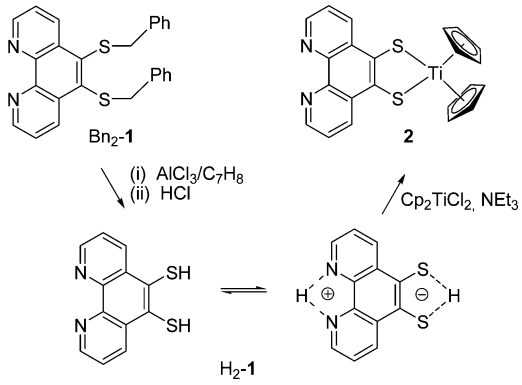

including single-crystal X-ray diffraction (Figure 1). The bonding parameters including the envelope structure of the

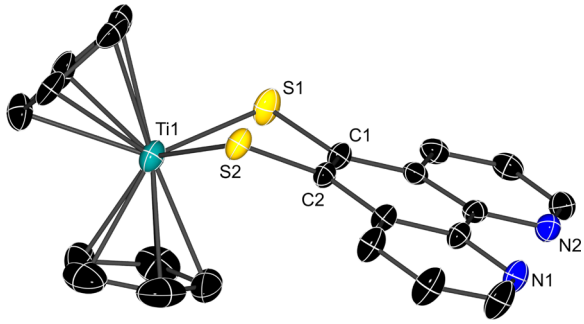

Figure 1. Molecular structure of **2** in the crystal with thermal ellipsoids set at 40% probability. Hydrogen atoms have been omitted for clarity. Selected bond lengths [Å] and angles [°]: Ti1−S1 2.417(1), Ti1−S2 2.391(1), C1−S1 1.752(4), C2−S2 1.741(4), C1−C2 1.387(5), C1−C2−S2 121.3(3), C2−C1−S1 119.9(3), S1−S2 3.170(2), S1−Ti1−S2 82.5(4).

chelate ring (folding about the S−S axis 44.24°) match those of related complexes[32] like $[(C_5H_5)_2Ti(S_2C_6H_4)]$. No $\pi-\pi$ interactions are observed between adjacent phen planes (plane angle 86.2°). Unfortunately, all attempts to form dinuclear complexes with Ru(II) or Ir(III) resulted in an untimely cleavage of the titanocene moiety.

Therefore, we changed our strategy and prepared *N,N′*-phenanthroline complexes at first and removed the thiol protective groups subsequently (Scheme 2). We chose the cyanoethyl protective group, which can be removed with *tert*-BuOK leading to acrylonitrile and the desired potassium thiolato salt. The derivative $(NC-C_2H_4)_2$-**1**, **3**, is easily accessible in large scale according to Hudhomme et al.[14] However, the use of DMF as solvent as described by Zuo et al.[33] and others allows for a simple nucleophilic substitution of sodium 2-cyanoethylthiolate for the bromido substituents in Br_2phen at ambient temperature and without need of any catalyst. The phenanthroline-5,6-disulfide **3** was isolated analytically pure by column chromatography and characterized by ^{1}H and ^{13}C NMR spectroscopy. Derivative **3** revealed to be a reliable starting material in the formation of Ru(II) and Ir(III) complexes using published procedures.[14,34,35] The Ru(II) complex $[(C_5H_5)Ru(PPh_3)(N,N'$-**3**$)](PF_6)$, **4**-PF_6, was obtained straightforwardly from $[(C_5H_5)Ru(PPh_3)(CH_3CN)_2]$-$(PF_6)$. The Ru(II) complex $[(bpy)_2Ru(N,N'$-**3**$)](PF_6)_2$, **5**-$(PF_6)_2$, and the Ir(III) complex $[(ppy)_2Ir(N,N'$-**3**$)](PF_6)$, **6**-

dx.doi.org/10.1021/ic4031206 | Inorg. Chem. 2014, 53, 8859−8873

Scheme 2. Synthesis of Dinuclear Phendt^{2-} Complexes: (i) [(dppe)NiCl$_2$]; (ii) [(dppe)NiCl$_2$ or (dppv)NiCl$_2$; (iii) [(phen)PtCl$_2$]

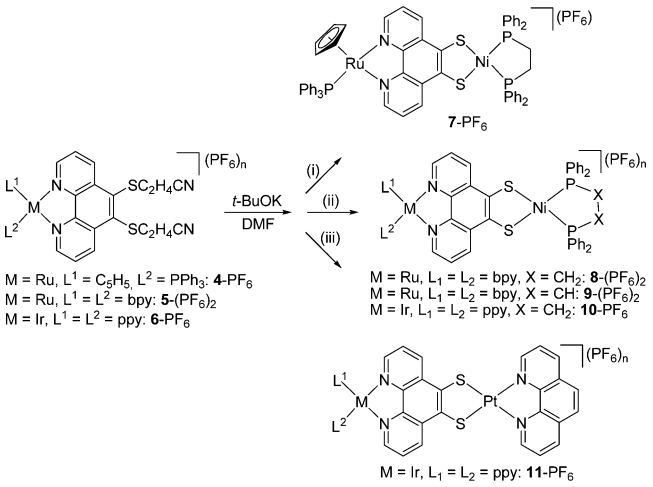

PF_6, were obtained using either $[(bpy)_2RuCl_2]\cdot 2\ H_2O$ in refluxing ethanol or $[(ppy)_2IrCl]_2$ at room temperature, respectively, after addition of aqueous KPF_6 to ethanolic solutions. All complex cations were detected by ESI mass spectrometry and conclusively characterized by NMR spectroscopy. The unequivocal assignment of aromatic signals is based on 2D NMR methods (Figures S1−S11). As expected, coordination of the Ru(bpy)$_2$ and Ir(ppy)$_2$ moiety led to a high field shift of the phen proton at 2-position (9.22 ppm in **3** to 8.53 ppm in $\mathbf{5}^{2+}$ and to 8.36 ppm in $\mathbf{6}^{+}$). Interestingly, the opposite is observed for the $(C_5H_5)(Ph_3P)Ru$ complex $\mathbf{4}^{+}$ with the corresponding resonance being observed at 9.61 ppm. Accordingly, the downfield shift of approximately 0.4 ppm induced by coordination is overcompensated by the highfield shift of about 1.2 ppm due to the anisotropy effects in the polypyridine complexes $\mathbf{5}^{2+}$ and $\mathbf{6}^{+}$. As an example, the identity of complex **6**-PF_6 was proven by X-ray diffraction analysis (Figure 2). Complex $\mathbf{6}^{+}$ displays the expected distorted octahedral coordination with *trans* configuration of the pyridine

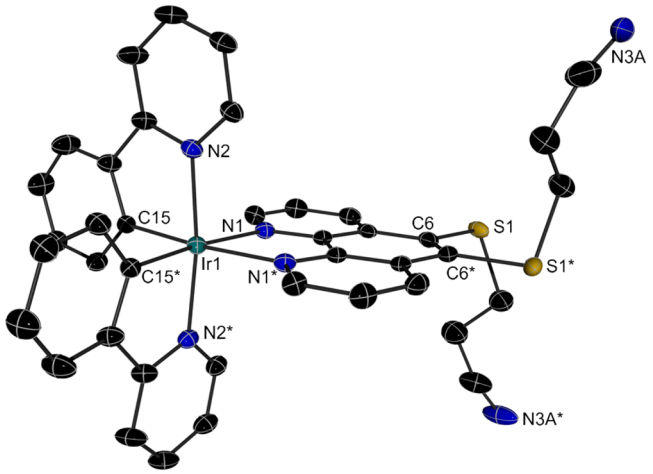

Figure 2. Molecular structure of $\mathbf{6}^{+}$ in the crystal with thermal ellipsoids set at 50% probability. Hydrogen atoms have been omitted for clarity. Selected bond lengths [Å] and angles [°]: Ir1−C15 2.009(3), Ir1−N1 2.137(3), Ir1−N2 2.048(3), C6−S1 1.812(4), C6−C6*1.375(9), C6*−C6−S1 121.92(14), S1−S1* 3.292(2).

N atoms. The C6−S1 bond distance of 1.812(4) Å is significantly larger as compared with the titanocene dithiolate complex **2** displaying C1−S1 and C2−S2 values of 1.752(4) and 1.741(4) Å, respectively. Accordingly, the large bite angle indicated by an intramolecular *S*,*S*′ distance of 3.292(2) Å in $\mathbf{6}^{+}$ is substantially reduced in the dithiolato complex **2** with 3.169(2) Å.

According to Scheme 2 complexes **4**-PF_6 to **6**-PF_6 allow removal of the cyanoethyl groups by *tert*-BuOK in DMF without decomposition of the complex core. Subsequently, the resulting anionic or neutral products were directly reacted with $[Ni(dppe)Cl_2]$ {dppe = $C_2H_4(PPh_2)_2$}, $[Ni(dppv)Cl_2]$ {dppv = $C_2H_2(PPh_2)_2$} or $[Pt(phen)Cl_2]$. The crude products are subjected to chromatographic purification leading to the pure dinuclear complexes **7**-PF_6 to **11**-PF_6. ESI mass spectrometry revealed the correct masses of the complex cations, whereas elemental analyses confirmed the overall complex composition. In addition, the ^{31}P NMR resonances at 60.0 ppm for **8**-$(PF_6)_2$ and **10**-(PF_6), and at 68.0 ppm for **9**-$(PF_6)_2$ are observed in the expected range. In ^{1}H NMR, the phen protons at 2- and at 4-position serve as a probe for the dithiolate coordination of Ni(II) or Pt(II) by significant highfield shifts, which amount to 0.6 to 0.7 ppm for the protons at 4-position and to 0.45 for that at 2-position (Figure S10). Although all complexes are obtained in crystalline form from solution, solely single crystals of **7**-PF_6 allowed a satisfying structure elucidation by X-ray diffraction analysis. A related X-ray diffraction experiment with the Ir/Ni complex **10**-PF_6 can at least serve as a proof of identity (Figure S13). The molecular structure of the complex cation $\mathbf{7}^{+}$ is depicted in Figure 3, and metrical parameters are given in the figure caption.

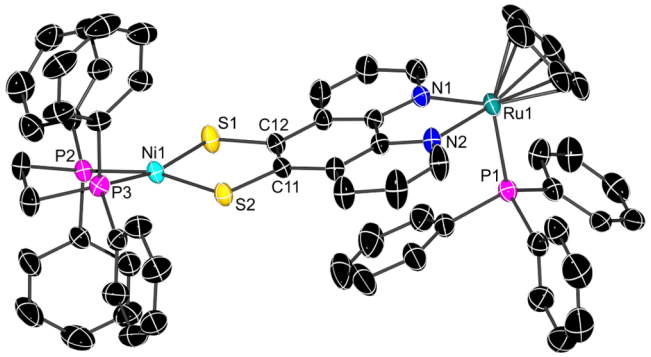

Figure 3. Molecular structure of $\mathbf{7}^{+}$ in the crystal with thermal ellipsoids set at 50% probability. Hydrogen atoms have been omitted for clarity. Selected bond lengths [Å] and angles [°]: Ru1−P1 2.3010(7), Ru1−N1 2.0723(19), Ru1−N2 2.1007(18), Ni1−S1 2.1517(6), Ni1−S2 2.1572(6), Ni1−P2 2.1659(6), Ni1−P3 2.1516(6), C11−S2 1.746(2), C12−S1 1.744(2), C11−C12 1.369(3), S1−Ni−S2 92.30(2), P2−Ni−P3 86.76(2).

The solid state structure of complex $\mathbf{7}^{+}$ proved unambiguously the μ−κ^2-*N*,*N*′-κ^2-*S*,*S*′-coordination mode of phendt^{2-} coordinating Ru(II) by the diimine chelate and Ni(II) by the dithiolate moiety. The latter NiS_2 core of $\mathbf{7}^{+}$ resembles related group 10 ene-1,2-dithiolate complexes.[36] The Ni−S1 and Ni−S2 bond lengths are on the short end of range for Ni(dppe)dithiolate complexes, whereas the C11−C12 bond and the C11−S2/C12−S1 bonds represent double and single bonds, respectively, underscoring the ene-1,2-dithiolate character of the bridging phendt ligand in $\mathbf{7}^{+}$. However, the C11−S2

dx.doi.org/10.1021/ic4031206 | Inorg. Chem. 2014, 53, 8859−8873

and C12−S1 distances are again distinctively shorter compared to the cyanoethyl derivative $\mathbf{6}^{+}$. In addition, the dithiolene chelate ring plane, which is literally planar, and the Ni1−P2−P3 plane show a twist angle of 18.38°, indicating a distinct distortion from the square planar coordination at Ni. The intermetallic Ni1/Ru1 distance amounts to 8.29 Å.

UV−vis Absorption Spectroscopy. Generally, comparison of the UV−vis absorption spectra of the mono- and dinuclear complexes, respectively, shows that the predominant features are associated with the Ru or Ir chromophore. However, a closer inspection of the spectra provides some insight in contributions from both complex centers (Figure 4).

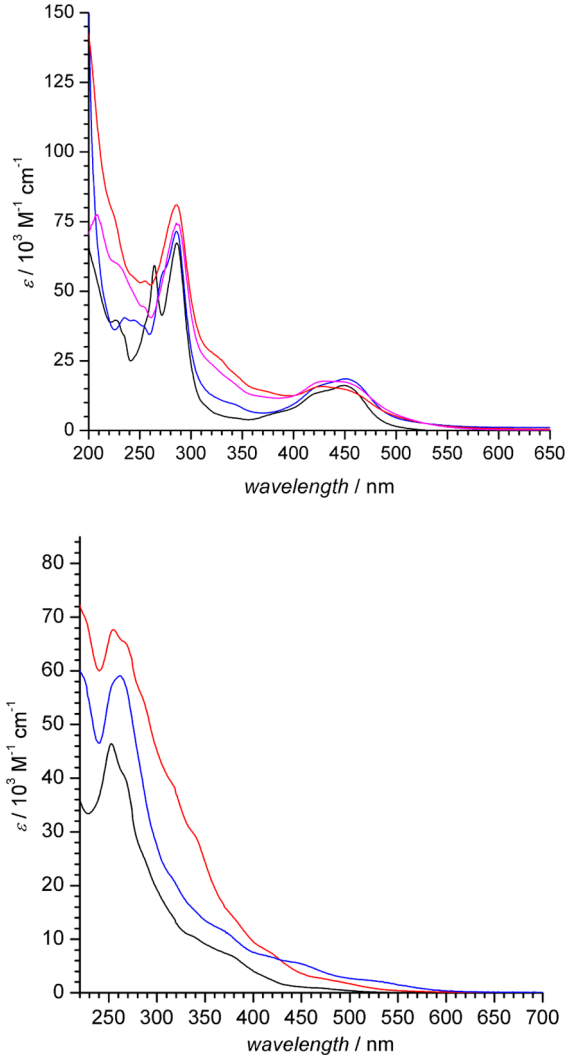

Figure 4. UV−vis absorption spectra. Top: $[Ru(bpy)_2(phen)]^{2+}$ (black), $\mathbf{5}^{2+}$ (blue), $\mathbf{8}^{2+}$ (red), $\mathbf{9}^{2+}$ (magenta); bottom: Ir complexes $\mathbf{6}^{+}$ (black), $\mathbf{10}^{+}$ (red) and $\mathbf{11}^{+}$ (blue); all complexes are PF_6^- salts dissolved in CH_3CN.

Assignment of the absorption bands can be carried out in analogy to a multitude of published $Ru(bpy)_2$ and $Ir(ppy)_2$[37] complexes and associated TD-DFT calculations.[4,16,34] In the visible range, the spectra of the mononuclear Ru(II) complex **5**-$(PF_6)_2$ and even the dinuclear Ru(II)/Ni(II) complex **8**-$(PF_6)_2$ exhibit a high similarity with the spectrum of the prototype complex $[Ru(bpy)_2(phen)](PF_6)_2$, indicating a restricted influence of substitution in 5,6-position on the electronic structure of phenanthroline. However, the two bands associated with metal-to-ligand-charge transfer (MLCT) transitions to bpy and the phen-type ligand, respectively, swap the intensity maxima going from mononuclear $[Ru(bpy)_2(phen)](PF_6)_2$ and **5**-$(PF_6)_2$ (450 nm) to dinuclear **8**-$(PF_6)_2$ (425 nm). The UV range of the spectra is dominated by spin allowed ligand centered (^{1}LC) π,π^* transitions at 286 nm, whereas two such high energy bands are observed for $[Ru(bpy)_2(phen)](PF_6)_2$. In comparison with the phen complex, the absorption bands are broader for all sulfur-substituted derivatives at the low energy slope, which is attributed to conjugation effects with sulfur lone pairs of **3**. The additional intensity increase for the dinuclear complex **8**-$(PF_6)_2$ in the 300 to 400 nm range (weak shoulder at 330 nm) is probably caused by underlying CT transitions associated with the bridging ligand $\mathbf{1}^{2-}$ (vide infra). Similar conclusions were drawn for a related dinuclear Ru−Ni-complex with a phenanthroline diimine-Schiff base bridging ligand.[38]

In comparison, the UV−vis absorption spectra of the Ir(III) complexes depicted in Figure 4 are relatively featureless, which can be attributed to a blue shift of the MLCT bands because of the higher energy of the phendiyl groups and an increased manifold of accessible transitions as a result of the stronger spin−orbit coupling of Ir(III). Consequently, the absorptivity in the visible region is weak compared to related Ru(II) polypyridine systems. One strong absorption band with maxima at 252 nm (**6**-PF_6) and 255 nm (**10**-PF_6) extends to approximately 500 nm with shoulders of decreasing absorptivity. The predominant description is based on the assignment of three absorption regions: (i) spin-allowed ligand centered (^{1}LC) transitions between 240 and 280 nm, (ii) less intense absorption shoulders in the region of 280 to 430 nm, attributed to spin-allowed ^{1}MLCT transitions with increasing π,π^* mixing with increasing energy, and (iii) weak absorptions around 450 to 520 nm attributed to spin-forbidden ^{3}MLCT transitions. Comparison of the spectra of mononuclear **6**-PF_6 and **10**-PF_6 reveals a distinct intensity increase in the near UV and blue spectral range for the latter. In addition, the low energy tail of the spectra of **10**-PF_6 is red-shifted by ca. 3000 cm^{-1} to 600 nm. These observations point to some electronic interaction between the Ir complex core and the Ni-complex moiety as similarly concluded above for the Ru/Ni complex **8**-$(PF_6)_2$.

However, relating to the extension of the low energy range in the dinuclear complexes, the appearance of bands corresponding to d−d or dithiolate S-π to phen π^* transitions, that were reported for related Ni(dppe) dithiolate complexes[39] at about 600 nm with very low extinction coefficients (ca. 100 M^{-1} cm^{-1}), has to be considered. The absorption spectra of $\mathbf{10}^{+}$ in $CHCl_3$ reveal in contrary to those of $\mathbf{6}^{+}$ a small band with a maximum of about 200 M^{-1} cm^{-1} at 595 nm (Figure S23). In CH_3CN and CH_2Cl_2, no such pronounced absorption band was observed, but an extension of the red wing and a slight absorption increase in the region 550 to 650 nm were observed. The existence of such d-d or dithiolate S-π to phen π^* transition is further supported by the absorption spectrum of the Pt complex **11**-PF_6 in acetonitrile, which clearly shows a shoulder at 530 nm matching the absorption of 583 nm reported for [(phen)Pt(tdt)] (tdt = toluenedithiolate) in dichloromethane and the solvatochromic behavior of this charge transfer band.[40] Thus, the respective redshift of the low energy transitions going from mononuclear **6**-PF_6 to **10**-PF_6 might be attributed to such transitions in the Ni complex core. In addition, for the Ru complex pair **5**-$(PF_6)_2$ and **8**-$(PF_6)_2$, some mixing of Ni into the relevant frontier orbitals of the Ru

dx.doi.org/10.1021/ic4031206 | Inorg. Chem. 2014, 53, 8859−8873

phenanthroline chromophore is evident by the influence of the particular phosphane ligand at Ni on the individual spectra. Although the dppe complex $\mathbf{8}^{2+}$ shows below 405 nm a slightly higher intensity compared to the dppv complex $\mathbf{9}^{2+}$, the opposite holds true above that intersection (Figure 4, top).

Luminescence Behavior. Steady state emission spectroscopy in solution revealed for both, mono- and dinuclear complexes with $Ru(bpy)_2$- and $Ir(ppy)_2$-moieties a red photoluminescence at ca. 620 nm in acetonitrile (Figure 5a).

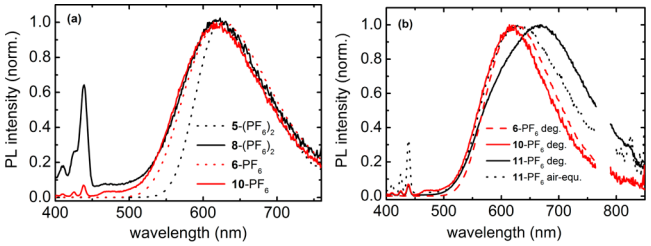

Figure 5. Normalized emission spectra ($I(\lambda_{max}) = 1$) for (a) **5**-$(PF_6)_2$, **8**-$(PF_6)_2$, **6**-PF_6 and **10**-PF_6 in degassed CH_3CN, and (b) for **6**-PF_6, **10**-PF_6, **11**-PF_6 in degassed CH_3CN, and **11**-PF_6 in air-equilibrated CH_3CN.

Effective quenching by O_2 supports a ^{3}MLCT emissive state, which is characteristic for complexes of this type. The determined quantum yield for the Ru complex **5**-$(PF_6)_2$ of 0.13 and the PL lifetime of 2.3 μs are relatively large compared to many other Ru-complexes.[41] However, there are also a few examples exhibiting similar or even higher quantum yields and they are also accompanied by relatively long lifetimes of up to 2.5 μs.[42] For the dinuclear complexes, a substantial luminescence quenching is observed related to the mononuclear ones. Remarkably, the PL intensity quenching is more effective by a factor of about 20 in the Ru/Ni complex **8**-$(PF_6)_2$ as compared with the Ir/Ni complex **10**-PF_6. The quantum yield φ_{PL} of 0.091 for **6**-PF_6 in degassed CH_3CN (Table 2) is significantly reduced in the dinuclear complexes **10**-PF_6 and **11**-PF_6 to 7% and 8% of its original value, respectively. However, the quantum yields of the Ru complexes **5**-$(PF_6)_2$ and **8**-$(PF_6)_2$ under the same conditions are at a ratio of 0.13 to 0.0005. Hence, only 0.4% of the primary luminescence is observed in the dinuclear Ru/Ni complex.

Variation of the solvent polarity with the mononuclear complex **6**-PF_6 resulted only in a slight shift of the luminescence maximum (Table 2 and Figure S21) and an increase of quantum yield φ_{PL} from 0.091 in CH_3CN to 0.20 in CH_2Cl_2. Dinuclear **10**-PF_6 exhibits a similarly slight solvent dependence and a marginal solvent influence on the quantum yield ratio **10**-PF_6/**6**-PF_6 of 7%. The obvious quenching effect on the emission by the sulfur coordinated Ni atom can alternatively be attributed either to an electron transfer, an energy transfer or a substantial change of the CT states.

To get insight into the quenching mechanism, time-resolved photoluminescence measurements were performed. The lifetimes for the emission band of the mononuclear complex **6**-PF_6 in different solvents (Table 2, e.g., τ_{PL} = 490 ns in CH_3CN) match those of related $Ir(ppy)_2$ complexes. However, the dinuclear Ir/Ni complex **10**-PF_6 shows surprisingly a comparable lifetime (τ_{PL} = 440 ns in CH_3CN). Hence, the thermally equilibrated excited state responsible for the emission in dinuclear **10**-PF_6 is obviously separated from the deactivation channel causing the photoluminescence quenching. Test series with mixtures of **6**-PF_6 and **10**-PF_6 proved the genuine emission of **10**-PF_6 and ruled out, that the residual emission of **10**-PF_6 might be traced back to impurities of **6**-PF_6 (Figures S15 and S16). The similarity of the determined lifetimes and the difference in quantum yields disclose the existence of a second, much faster deactivation channel. According to the time resolution used in our experiments, the deactivation process proceeds with a time scale <200 ps ($k > 5 \times 10^9$ s^{-1}). In contrast, the lifetime of the dinuclear Ru/Ni complex **8**-$(PF_6)_2$ with τ_{PL} = 400 ns in CH_3CN (Table 2 and Figure S18) is considerably decreased related to the mononuclear complex **5**-$(PF_6)_2$ with τ_{PL} = 2.3 μs. This observation is nicely reflected by the higher intensity quenching efficiency of the Ni center in the Ru complex as compared to the Ir complex.

The Pt(II) phen complex **11**-PF_6 was synthesized with the idea in mind that according to investigations by Eisenberg Pt diimindithiolato complexes, in contrast to corresponding Ni complexes, are known to show emission in solution.[40] If the photoluminescence quenching in **10**-PF_6 is based on a very fast triplet triplet energy transfer by the Dexter mechanism, the Pt(II) complex might show emission from a platinum based excited triplet state. Steady state luminescence measurements with **11**-PF_6 show indeed an additional red emission band II

Table 2. Photoluminescence Maxima, Lifetimes, and Quantum Yields for the Mono- and Dinuclear Ru and Ir Complexes 5-$(PF_6)_2$, 8-$(PF_6)_2$, 6-PF_6, and 10-PF_6, and Maxima and Quantum Yields of 11-PF_6 (λ_{exc} = 388 nm)

	λ_{max}	τ_{PL}	φ_{PL}		λ_{max}	τ_{PL}	φ_{PL}
5-$(PF_6)_2$				**8**-$(PF_6)_2$			
CH_3CN (deg.)	625 nm	2.3 μs (±0.2 μs)	0.13 (±0.02)		620 nm	400 ns (±40 ns)	0.0005 (±0.00006)
CH_3CN (air-equ.)		165 ns (±20 ns)	0.010 (±0.001)			80 ns (±10 ns)	0.00009 (±0.00001)
6-PF_6				**10**-PF_6			
$CHCl_3$ (deg.)	615 nm	640 ns (±60 ns)	0.17 (±0.02)		600 nm	650 ns (±70)	0.011 (±0.002)
$CHCl_3$ (air-equ.)		160 ns (±15 ns)	0.043 (±0.005)			150 ns (±15 ns)	0.004 (±0.001)
CH_2Cl_2 (deg.)	615 nm	660 ns (±70 ns)	0.20 (±0.03)		605 nm	715 ns (±70)	0.014 (±0.002)
CH_2Cl_2 (air-equ.)		185 ns (±20 ns)	0.053 (±0.006)			185 ns (±20 ns)	0.004 (±0.001)
CH_3CN (deg.)	625 nm	490 ns (±50 ns)	0.091 (±0.014)		620 nm	440 ns (±40 ns)	0.0064 (±0.0007)
CH_3CN (air-equ.)		80 ns (±10 ns)	0.015 (±0.002)			65 ns (±10 ns)	0.0009 (±0.0002)

	λ^{I}_{max}	λ^{II}_{max}	φ^{I+II}
11-PF_6			
CH_3CN (deg.)	~625 nm (sh)	670 nm	0.0072 (±0.0008)
CH_3CN (air-equ.)	625 nm		0.0012 (±0.0003)

dx.doi.org/10.1021/ic4031206 | Inorg. Chem. 2014, 53, 8859−8873

with a maximum of 670 nm (Table 2, Figure 5b). The maximum of the emission band I for **11**-PF_6 apparent by a shoulder at 625 nm in degassed CH_3CN remains practically unaltered compared with mononuclear **6**-PF_6 and the Ni(dppe) system **10**-PF_6. Thus, the red emission band II at 670 nm originates most likely from the Pt chromophore. For the related mononuclear complex [Pt(phen)(tdt)] (tdt = toluenedithiolate) an emission of 674 nm at 77 K (C_3H_7CN) and of 730 nm in CH_2Cl_2 solution with φ_{PL} of 0.00067 was reported.[40] In air-equilibrated CH_3CN solution the emission spectrum of **11**-PF_6 is dominated by the 625 nm Ir originated emission band, revealing an obviously stronger O_2 quenching effect for the 670 nm emission band.

Electrochemistry. Electrochemical characterization was performed in order to determine the excited state redox potentials. Generally, cyclic voltammetry of the mononuclear complexes **4**-PF_6 to **6**-PF_6 and the dinuclear complexes **7**-PF_6 to **11**-PF_6, respectively, display a similar behavior (Figure 6).

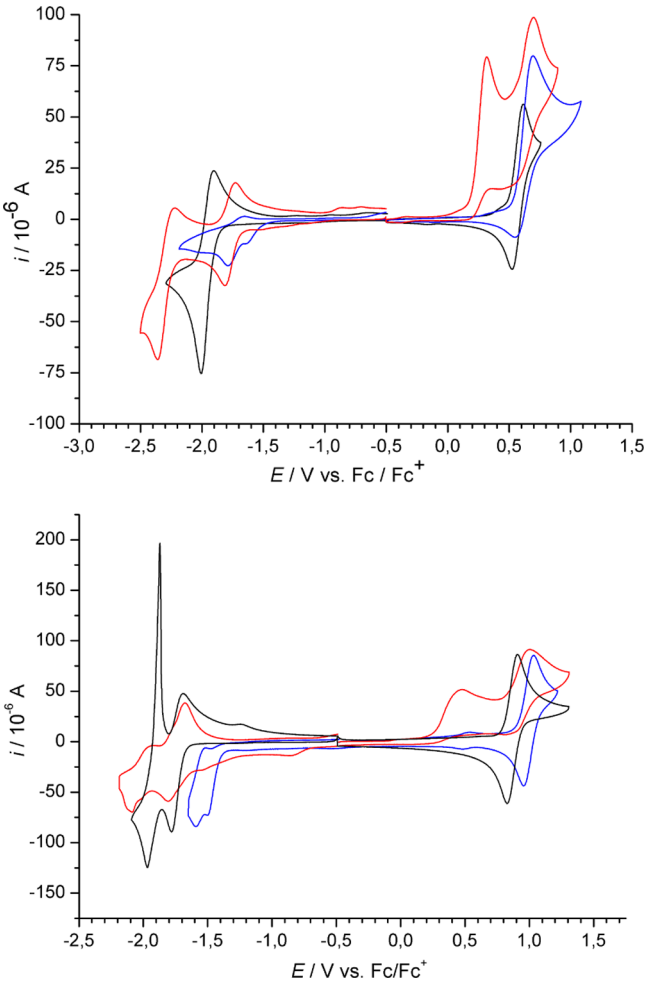

Figure 6. Cyclic voltammetry. Top: $[CpRu(PPh_3)(phen)]^+$ (black), $\mathbf{4}^+$ (blue) and $\mathbf{7}^+$ (red); bottom: $[Ru(bpy)_2(phen)]^{2+}$ (black), $\mathbf{5}^{2+}$ (blue), $\mathbf{8}^{2+}$ (red), all are PF_6^- salts and were measured in CH_3CN.

The oxidation and reduction potentials are given in Table 3. For all the complexes the first reduction in the range −1.7 to −2.0 versus Fc is due to reduction of the phenanthroline system. The $E_{1/2}$ values of the Ni(dppe) complexes $\mathbf{7}^+$, $\mathbf{8}^{2+}$, and $\mathbf{10}^+$ are nearly identical, whereas the alternative reduction of the Ni center is excluded by EPR spectroscopic evidence. Reduction of $\mathbf{8}^{2+}$ by Na-naphthalide in THF afforded paramagnetic $\mathbf{8}^+$. The X-band EPR spectrum in methyl-THF glass at 77 K shows one broad signal, which is best simulated with a slight anisotropy ($g_{\|}$ = 1.988 and $g_{\perp}$ = 2.002, Figure S12). The weak g value anisotropy and the lack of hyperfine coupling to phosphorus rule essential contributions of Ni out.[43] Unfortunately, for the mononuclear complexes with the neutral ligand **3**, the determination of $E_{1/2}$ values is impeded, because the signals are irreversible. This behavior can be attributed to the reductive removal of the cyanoethyl groups under these conditions.

In contrast, the first oxidation process, which is assigned to the oxidation of the metal centers Ru^{II}/Ru^{III} and Ir^{III}/Ir^{IV}, gives rise to reversible signals for the mononuclear complexes at +0.57 to +0.99 V versus Fc. In the cyclic voltammetry of the dinuclear complexes **7**-PF_6 to **11**-PF_6, an additional oxidation process is observed at lower potential (+0.32 to +0.48 mV vs Fc). These processes are irreversible in the cyclic voltammetry time scale, rendering the following original oxidation of the metal centers (Ru, Ir) irreversible as well. Because these processes are observed exclusively in the dinuclear complexes, this oxidation is assigned to the metal dithiolate moiety.

The excited state potentials were calculated using the well-defined $E_{1/2}$ values of the dinuclear complexes for the ligand reduction and of the mononuclear complexes for the Ru/Ir oxidation as well as the zero−zero energy E_{00} values. E_{00} was obtained here either from the intersection of absorption and emission spectra at room temperature or from the maximum of low temperature emission spectra (Figure S22, Table S1). The E_{00} value of 2.33 eV (532 nm) for **6**-PF_6 is very similar to E_{00} for the related Ir(III)-complex $[(ppy)_2Ir(bpy)]PF_6$ (2.36 eV),[44] and hence it is also used as an estimate for **10**-PF_6. Thus, the resulted excited state potentials amount to +0.61 and −1.46 V. The smaller E_{00} value of 2.26 eV (549 nm) for the Ru complexes **5**-$(PF_6)_2$ and **8**-$(PF_6)_2$ lead to the respective potentials of 0.52 and −1.27 V. Comparison with the ground state potentials of **8**-$(PF_6)_2$ and **10**-PF_6 discloses an electron transfer from the ^{3}MLCT thermally equilibrated excited state to be debatable. Particularly, it must be taken into account that the oxidation potential of the NiS_2 complex moiety is not well-defined due to the irreversible CV signal. Comparison of E^* = −1.46 V for **6**-PF_6 representing the reducing power of the photoactivated Ir^{IV}-$phen^-$ system with redox potentials of related $[Ni(dppe)(dithiolate)]^{0/-1}$ complexes ($E \sim -2.3$ V) render an electron transfer to the Ni complex moiety impossible. In contrast, the reverse electron transfer in **10**-PF_6 is much more likely, because the potentials of E^* = +0.61 V representing the oxidation power of photoactivated Ir^{IV}-$phen^{\cdot-}$ and the ground state potential of E = +0.45 V for **10**-PF_6 are comparable. However, an exergonic electron transfer from the Ni dithiolate moiety to Ir/Ru can be neither taken for granted nor excluded by the available electrochemical data.

Electronic Structure. Studies on the electronic structure and prediction of the vertical transition energies by density functional theory (DFT) and TD-DFT calculations are a challenge because of the strong spin orbit coupling of Ir and as a result of the presumable coupling of two metals. Because several theoretical investigations on $[(ppy)_2Ir(phen)]$ type complexes have already appeared,[16,34,45] we focus on the effect of Ni coordination at the dithiolate unit on the electronic structure at the Ir chromophore and the bridging ligand itself. Accordingly, we compare the dinuclear cation $\mathbf{10}^+$ with $[(ppy)_2Ir(H_2\text{-}\mathbf{1})]^+$, $\mathbf{6a}^+$, serving as a C_2 symmetric model for

dx.doi.org/10.1021/ic4031206 | Inorg. Chem. 2014, 53, 8859−8873

Table 3. Redox Potentials (V vs Fc/Fc^+) Measured in CH_3CN[a]

	$E_{1/2}$ (ground state)		E^* (excited state)	
	reduction	oxidation	reduction[b]	oxidation[c]
$[(C_5H_5)(PPh_3)Ru(phen)](PF_6)$	−1.96	+0.57		
4-PF_6		+0.62		
7-PF_6	−1.77	(+0.32)		
$[(bpy)_2Ru(phen)](PF_6)_2$	−1.73	+0.86		
5-$(PF_6)_2$	(−1.49)	+0.99		−1.27 (−1.12)
8-$(PF_6)_2$	−1.74	(+0.47)	+0.52 (+0.38)	
$[(ppy)_2Ir(phen)](PF_6)$	−1.76	+0.88		
6-PF_6	(−1.52)	+0.87		−1.46 (−1.52)
10-PF_6	−1.72	(+0.45)	+0.61 (+0.61)	
11-PF_6	(−1.20)	(+0.48)		

[a]Values in brackets indicate irreversible signals and represent peak potentials at 100 $mV \cdot s^{-1}$ scan rate. [b]$E^*(Ru^{II*/L-}) = E_{1/2}(Ru^{II/L-}) + E_{00}$. [c]$E^*(Ru^{III/II*}) = E_{1/2}(Ru^{III/II}) - E_{00}$; ($E_{00}$ determined by the interception method, in brackets: E_{00} determined from the low temperature spectra).

Table 4. Energies (E in eV)[a] and Composition (%)[b] of Frontier Molecular Orbitals of $6a^+$ and of the Ir/Ni complex 10^+

	$6a^+$				10^+					
	E	Ir	ppy	H_2-**1**	E	Ir	ppy	$C_{10}H_6N_2$	C_2S_2	Ni
L+3	−2.91	4.01	95.26	0.73	−2.32	3.62	93.43	2.26	0.61	0.01
L+2	−3.00	4.23	94.54	1.23	−2.42	3.96	92.97	1.26	0.39	0.70
L+1	−4.00	1.30	0.00	98.70	−2.66	2.07	1.92	73.06	21.55	0.36
L	−4.08	2.50	0.60	96.90	−2.99	2.41	0.84	95.14	1.61	0.00
H	−9.33	32.82	65.50	1.68	−8.31	0.28	0.06	16.3	73.68	3.86
H−1	−9.94	3.77	95.22	1.00	−8.71	34.92	63.33	1.74	0.01	0.00
H−2	−10.17	11.77	87.51	0.72	−9.24	0.09	0.18	17.62	62.12	19.81
H−3	−10.27	19.85	59.81	20.34	−9.36	4.66	94.49	0.74	0.06	0.02

[a]CAM-b3lyp functional. [b]Mulliken population analysis (MPA).

6^+. To account for the pronounced CT character of the transitions we used the functionals CAM-b3lyp[23] and lc-blyp[24] with corrections for the coulomb interaction. The accuracy of the geometry description is raised going from b3lyp over CAM-b3lyp to the lc-blyp functional (deviations 1.4 to 3.1%, 0.9 to 2.1%, and 0.2 to 0.6%, respectively, relating to all Ir−N bond lengths, Table S2).

As expected, the frontier orbitals of $6a^+$ (Figures S24 and S25) resemble those of $[(ppy)_2Ir(phen)]^+$ and related systems with HOMO and HOMO−n (n = 1−3) displaying a major contribution from the phendiyl π orbitals and a smaller proportion of Ir(5d) orbitals, whereas LUMO and LUMO+1 represent π^* orbitals of phen (Table 4). Thiol substitution at the 5,6-position decreases the HOMO/LUMO gap only marginally. Although the composition of the LUMO and LUMO+1 is almost unaltered in the dinuclear complex 10^+, the dithiolene moiety with the lone pairs at sulfur forms now the HOMO and the HOMO−2 penetrating the orbital scheme of the mononuclear complex leaving Ir-based HOMO−1 and HOMO−3 (Figures 7 and S25). As a consequence, the energy gap between the highest Ir-based orbital (HOMO in $6a^+$ and HOMO−1 in 10^+) and the LUMO is increased by 8.9% for 10^+. In contrast, the energy difference between the ppy-based LUMO+2 and the Ir-based HOMO ($6a^+$) or HOMO−1 (10^+), respectively, is slightly decreased in the dinuclear complex. In addition, inspection of the orbital contributions in Table 4 reveals a distinct separation of both complex centers. Although the contribution of the $Ir(ppy)_2$ moiety to the HOMO amounts to 0.28%, the corresponding share of the $C_2S_2Ni(dppe)$ moiety in the HOMO−1 adds up to 1.75%. A comparison of natural bond orbital (NBO) charges discloses significant differences between $6a^+$ and 10^+ solely for the S atoms (+0.042 and −0.301, respectively) and for the C atoms attached to it (−0.142 and −0.174, respectively). According to NBO analysis, the charge distribution in the Ir complex moiety is not affected by the coordination of a second divalent metal ion given an equal overall complex charge.

Subsequently, TD-DFT calculations with $6a^+$ and 10^+ were performed. As expected, the character of the different transitions is consistently MLCT, however, reflecting the covalent Ir−C bonds the charge-donating states are highly mixed with a substantial π-contribution of the phenyl system (see particularly HOMO−1, Table 4). Compared with the popular b3lyp functional, the calculated transitions for $6a^+$ are distinctively higher in energy by approximately 5500 cm^{-1} using the CAM-b3lyp (Tables S3 and S4) and by 10 000 cm^{-1} using the lc-lyp functional. The experimental maximum for 6^+ observed at 252 nm falls between the maxima of 272 nm calculated with CAM-b3lyp and of 235 nm obtained with lc-lyp (Figure S29). For the sake of clarity, the following discussion make use of the values obtained with the CAM-b3lyp functional; Table 5 comprises data of both for comparison. The singlet singlet transitions for $6a^+$ with HOMO to LUMO/LUMO+1 MLCT character are calculated to 405 and 363 nm, however, with very low oscillator strength f. The lowest strong transition with $f \geq 0.1$ at 335 nm is clearly associated with Ir to ppy MLCT. The respective singlet triplet transition energies encompass the range between 533 and 361 nm (lc-blyp) with a narrower scope calculated with the CAM-b3lyp functional.

According to similar results of Kühn et al. and others[46] on related Ir-based complexes, a reconsideration of the common assignment of bands was suggested. The weak bands in the range of 380−530 nm should rather be assigned to singlet triplet MLCT transitions, whereas the respective singlet singlet

dx.doi.org/10.1021/ic4031206 | Inorg. Chem. 2014, 53, 8859−8873

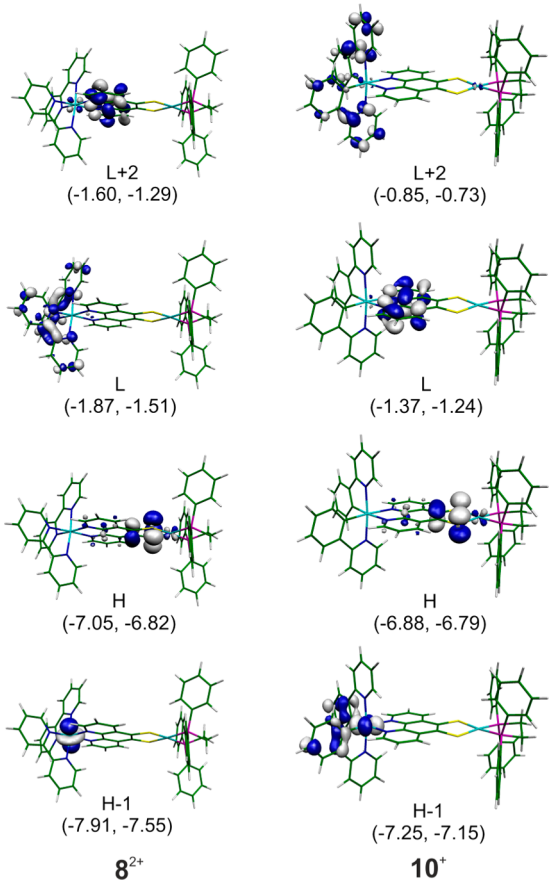

Figure 7. Essential frontier Kohn–Sham orbitals of the Ru complex $\mathbf{8}^{2+}$ (left) and the Ir complex $\mathbf{10}^{+}$ (right) using continuum solvent models; orbital energies (eV) in brackets (first number CH_2Cl_2, second number CH_3CN).

transitions are below the 388 nm limit used for irradiation in our luminescence measurements. This assignment is corroborated by the distinct decrease in absorptivity above 400 nm. However, the combination of TD-DFT with range separated functionals used provides apparently somewhat too high transition energies with the CAM-b3lyp seeming more appropriate.

Corresponding calculations with the dinuclear complex $\mathbf{10}^{+}$ revealed two essential facts. At first, the apparent increase of intensity observed between 300 and 400 nm going from mononuclear $\mathbf{6}^{+}$ to dinuclear $\mathbf{10}^{+}$ can be attributed to additional transitions, which are assigned to dithiolene-π to phen-π* ILCT transitions (Table 6). Particularly, the explicit HOMO to LUMO/LUMO+1 transitions calculated at 406 and 367 nm, fall in the range, which shows a significant intensity gain in the experimental UV–vis absorption spectrum of $\mathbf{10}^{+}$ compared with mononuclear $\mathbf{6}^{+}$. The MLCT transitions in the Ir chromophore identified for $\mathbf{6a}^{+}$ are only marginally affected by coordination of the second metal ion. For instance, the crucial Ir to ppy MLCT transition is calculated to 339 nm for $\mathbf{10}^{+}$ compared with 335 nm for $\mathbf{6a}^{+}$. The calculations did not deliver any evidence for transitions with metal metal CT character. Within the Ni complex moiety, S-π to Ni CT transitions are calculated to 500 nm and Ni d-d transitions to 477 nm, however, both with very small oscillator strength.

In order to get more information on the excited states, the lowest triplet state of $\mathbf{10}^{+}$ was calculated. Interestingly, using the optimized singlet geometry, we found a triplet state localized at the NiS_2 moiety to be the lowest in energy (Figure S26). Consideration of solvation (CH_3CN, polarized continuum model) as well as both solvation and anion contact (PF_6^-) did not have substantial influence on the character of this triplet state (Figure S27). A geometry optimization of this open shell triplet system resulted a tetrahedral coordination at Ni being 22.5 kcal/mol more stable compared with the triplet state at ground state geometry. In turn, this tetrahedral triplet state is calculated to be 18.5 kcal/mol less stable than the singlet ground state. A tetrahedral coordination geometry at Ni for the triplet state is in reasonable accordance with a simple ligand

Table 5. Selected Vertical Singlet Singlet and Singlet Triplet Transitions for $\mathbf{6a}^{+}$ As Calculated in Vacuo with Different Functionals, Assignment of the Transitions within the Kohn–Sham Orbital Scheme

	lc-blyp			CAM-b3lyp		
	λ/nm (f)[a]	dominant component(s)		λ/nm (f)[a]	dominant component(s)	CT-type
^{1}B	293 (0.18)	L+2←H (66%)	^{1}B	335 (0.10)	L+2←H (86%)	ppy←Ir
^{1}A	283 (0.08)	L←H−3 (30%)	^{1}A	333 (0.09)	L←H−3 (39%)	phen←Ir
		L←H−4 (37%)			L←H−4 (31%)	
^{1}B	276 (0.08)	L+1←H−3 (21%)	^{1}B	311 (0.10)	L+1←H−4 (52%)	phen←Ir
		L+1←H−4 (41%)			L+1←H−3 (27%)	
^{1}A	253 (0.14)	L←H−6 (62%)				phen←Ir
			^{1}A	274 (0.09)	L+2←H−1 (49%)	π*←π
^{1}B	239 (0.22)	L+2←H−2 (11%)	^{1}B	273 (0.09)	L+2←H−2 (28%)	ppy←Ir
		L←H−7 (15%)			L+3←H−1 (21%)	π*←π
^{1}A	234 (0.22)	L+1←H−5 (51%)	^{1}A	293 (0.06)	L+1←H−5 (62%)	phen←Ir
^{3}B	533	L+1←H−4 (34%)[b]	^{3}B	503	L+1←H−4 (42%)	phen←Ir
^{3}B	454	L+3←H−1 (22%)[b]	^{3}B	437	L+3←H−1 (25%)	ppy←Ir
		L+2←H (17%)[b]			L+2←H (30%)	
^{3}A	453	L+2←H−1 (28%)[b]	^{3}A	435	L+2←H−1 (34%)	ppy←Ir
		L+3←H (13%)[b]			L+3←H (23%)	
^{3}A	361	L←H−4 (22%)[b]	^{3}B	410	L←H (90%)	phen←Ir
		L←H−3 (20%)[b]				

[a]Limit $f \geq 0.05$. [b]Transitions are highly multi configurational.

dx.doi.org/10.1021/ic4031206 | Inorg. Chem. 2014, 53, 8859–8873

Table 6. Selected Vertical Singlet Singlet and Singlet Triplet Transitions for 10^+ As Calculated in Vacuo with Different Functionals, Assignment of the Transitions within the Kohn−Sham Orbital Scheme

	lc-blyp		CAM-b3lyp			
	λ/nm (f)[a]	dominant component(s)	λ/nm (f)[a]	dominant component(s)	CT-type
^{1}A	331(0.11)	L←H (88%)	^{1}A	406 (0.06)	L←H (96%)	phen←Sπ
^{1}B	315(0.07)	L+1←H (80%)	^{1}B	367 (0.06)	L+1←H (87%)	phen←Sπ
^{1}B	294 (0.16)	L+3←H−1 (69%)	^{1}B	339 (0.09)	L+2←H−1 (82%)	ppy←Ir
^{1}B	262 (0.12)	L←H−2 (45%)	^{1}B	306 (0.05)	L←H−2 (51%)	phen←Sπ
		L←H−6 (13%)			L←H−6 (21%)	phen←Ir
			^{1}A	292 (0.32)	L←H−5 (32%)	phen←Ir
^{1}A	254 (0.31)	L+1←H−2 (65%)				phen←Sπ
^{3}B	691	L+4←H−10 (47%)	^{3}B	902	L+4←H−9 (61%)	d←d (Ni)
^{3}B	553	L+1←H (59%)	^{3}B	543	L+1←H (76%)	phen←Sπ
			^{3}A	472	L←H (84%)	phen←Sπ
^{3}B	454	L+2←H−4 (17%)[b]				ppy←Ir
^{1}A	453	L+2←H−3 (27%)[b]				ppy←Ir

[a]Limit $f \geq 0.05$. [b]Transitions are highly multi configurational.

field consideration for a Ni(II), S = 1 system. In summary, although the most intense calculated singlet singlet transition in the Ir chromophore is of ppy ← Ir CT character the most stable triplet state of the system is located at the Ni complex core. These results are in full agreement with a Dexter energy transfer mechanism.

For comparison, related calculations were performed with the Ru complexes $[(bpy)_2Ru(H_2\text{-}\mathbf{1})]^{2+}$, $\mathbf{5a}^{2+}$, and $\mathbf{8}^{2+}$. The results are in line with published calculations on $[Ru(bpy)_3]^{2+}$ and particularly $[Ru(bpy)_2(phen)]^{2+}$.[47] The most striking difference between the Ir and the Ru complexes applies to the order and energy gaps between the lowest unoccupied orbitals. Although in the $[Ir(ppy)_2(phen)]^{2+}$ complexes, the phen π^* orbitals are lower in energy than the ppy π^*, the opposite holds true for bpy π^* and phen π^* in the $[Ru(bpy)_2(phen)]^{2+}$ complexes. Interestingly, this difference is most distinctive in the dinuclear complexes $\mathbf{8}^{2+}$ and $\mathbf{10}^+$ (Figure 7). In the Ru complex $\mathbf{8}^{2+}$, the LUMO and LUMO+1, which are bpy-based, lie approximately 0.25 eV lower in energy than the LUMO+2, which is phendt-based. As discussed above (Table 4), this is in clear contrast to the Ir complex $\mathbf{10}^+$. In accordance, spin density in the geometry optimized triplet state of the mononuclear Ru complex $\mathbf{5a}^{2+}$ is clearly located at Ru and the bpy ligand, whereas a strong contribution of the phen ligand H_2-**1** is evident in the corresponding Ir complex $\mathbf{6a}^+$ (Figure S28).

DISCUSSION

The UV−vis absorption measurements supported by related DFT calculations uncover a rather additive behavior of both complex centers in dinuclear phendt^{2-} complexes. This observation is in line with related dinuclear complexes with the shorter bis(pyrimidine) bridge with respect to the UV−vis absorption spectra, but it does not apply for the luminescence behavior.[48] For the Ir complexes, the salient result of our luminescence measurements is the inconsistency of a significant luminescence intensity quenching and the invariance of lifetimes for the corresponding emitting states going from mononuclear Ir to dinuclear Ir/Ni complex. Even though the 75% increase of absorptivity for **10**-PF_6 relative to **6**-PF_6 at 388 nm is attributed to Sπ to phen-π^* transitions, which do not lead to emissive states, the drop of quantum yields cannot be attributed solely to this effect. From this behavior, it can be inferred that the quenching mechanism interferes with the deactivation from the initially populated ^{1}MLCT or ^{3}MLCT to the final emitting $^3MLCT_2$ state (Figure 8). Accordingly, the

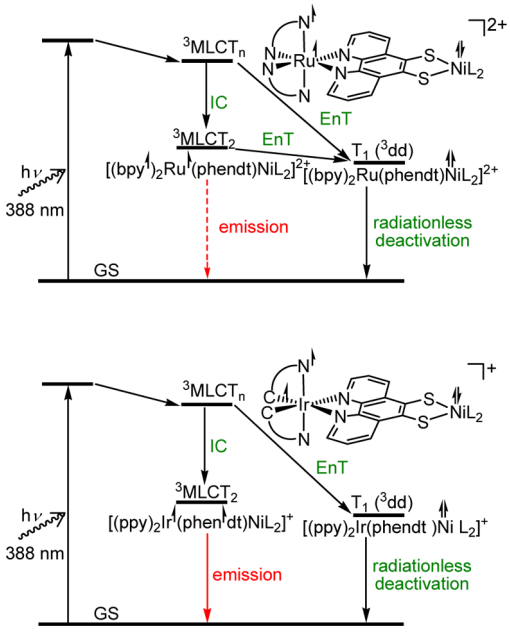

Figure 8. Qualitative energy diagram for charge transfer states in $\mathbf{8}^{2+}$ (top) $\mathbf{10}^+$ (bottom) upon excitation.

observed luminescence quenching for the dinuclear complex **10**-PF_6 to 7% of the value determined for the mononuclear Ir complex **6**-PF_6 is attributed to an effective energy transfer by the Dexter mechanism from higher $[Ir(ppy)_2(phendt)]$ to $[Ni(dppe)(phendt)]$ states. The latter are known to deactivate by nonradiation processes.[39] Low-temperature luminescence measurements at 90 K show only a partial luminescence recovery for the dinuclear complexes in butyronitrile glass relating to ambient temperature solution and the mononuclear prototypes (Figure S22). This behavior is rather consistent with a Dexter energy transfer. The time resolution of our luminescence measurements delivers a lower time limit of 200 ps for this energy transfer. Detailed examinations on the relaxation dynamics of related Ir complexes showed time limits

dx.doi.org/10.1021/ic4031206 | Inorg. Chem. 2014, 53, 8859−8873

of <1 ps for the intersystem crossing (ISC) and <10 ps for the $T_1 \leftarrow T_n$ conversion.[49] Similar observations of an incomplete luminescence quenching were reported by Eisenberg for related phenantholine diolate complexes as well as by Shatruk for a tetrathiafulvalene fused Ru phenathroline system.[16] In contrast, the Ru/Ni complex **8**-$(PF_6)_2$ exhibits a rather reasonable relation between strong quenching effect and determined excited state lifetime. Obviously, the energy transfer from the equilibrated ^{3}MLCT state to the Ni complex moiety is effective for M = Ru. The observed difference between the Ru/Ni and the Ir/Ni system cannot be traced back to their electrochemical behavior because the excited state redox potentials of the dinuclear Ru/Ni and Ir/Ni complexes do not show significant differences. In addition, the low temperature luminescence measurements are comparable for Ru/Ni and Ir/Ni complexes with E_{00} values being higher in energy for the latter. Finally, a completely different quenching mechanism like the population of ^{3}dd states as discussed by Hauser et al. for Ru(II) complexes[50] is unlikely, because the calculations do not provide any evidence of a drastic change of the diimine ligand field strength by coordination of Ni^{2+} on phendt. However, the different luminescence behavior of the $Ru(bpy)_2^{2+}$ and $Ir(ppy)_2^{+}$ could be attributed to differing orbital contributions to the emissive state. According to the frontier orbital ordering, the emissive state in the Ir complex $\mathbf{10}^+$ is predominantly localized at the phendt bridging ligand with the additional charge acting as a barrier for the energy transfer. A presumed localization of the emissive state on the bpy ligands in the Ru complex $\mathbf{8}^{2+}$ could serve as a rationale for an accessible energy transfer path.

An essential alteration of the electronic structure of the original ^{1}MLCT and ^{3}MLCT excited states in $\mathbf{6}^+$ by nickel dithiolate orbital contributions in $\mathbf{10}^+$ can be ruled out by the high similarity of UV−vis absorption spectra between mono- and dinuclear Ru(II) and Ir(III) complexes, respectively. This perception is supported by the results of TD-DFT calculations showing a restricted influence of the dithiolato bound Ni^{II} on the chromophore at Ir. In addition, we have no indication of any charge separation by a single electron transfer. A small influence of solvent polarity on the emission wavelength and particularly on the quantum yield is rather not consistent with changes of the molecular charge distribution associated with a single electron transfer. Furthermore, the notion of an energy transfer is consistent with the observation of an additional emission at 670 nm for the Ir/Pt complex **11**-PF_6. According to investigations by Eisenberg and Pilato this emission is typical for Pt dithiolate complexes. However, absorptions based on direct Sπ to phen-π^* transitions cannot be ruled out as a source for the additional emission observed. Attempts to isolate mononuclear Pt(II) dithiolato complexes with $\mathbf{1}^{2-}$ bearing a free diimine donor site in analogy to complex **2** serving as standard for quantitative measurements were not successful so far.

CONCLUSION

Dinuclear complexes with phenanthroline-5,6-dithiolate bridging different metals are easily accessible by a consecutive coordination strategy. The use of cyanoethyl protective groups at the thiol function allows coordination of Ru^{II} and Ir^{III} at the diimine donor unit. These mononuclear diimin complexes are stable enough to allow for removal of the cyanoethyl groups and subsequent coordination of a second metal like Ni^{II} or Pt^{II}. All dinuclear complexes are obtained in crystalline form and in high purity. The adaption of the facile procedure to various derivatives or metal combinations seems promising.

According to our photophysical and electrochemical investigations, the drastic drop of the luminescence quantum yield going from mononuclear Ru^{II} or Ir^{III} complexes to the dinuclear congeners can be attributed to a very fast Dexter energy transfer. Energy transfer from the equilibrated ^{3}MLCT state turned out to be more efficient in $[Ru(bpy)_2]$ than in $[Ir(ppy)_2]$ complexes. Reasonably, this difference can be attributed to a higher barrier in the Ir complex due to the predominant phendt-based emissive state. Generally, the ditopic ligand phenanthroline-5,6-dithiolate constitutes the basis for a very fast electron transfer path depending on the redox potentials of the metal complex fragments linked to it. Alternative complex units at the dithiolate like bis(dithiolene) moieties showing a redox potential between both limits given by the photoactivated complex center should allow the reduction of the *S*-coordinated metal. For such a system, a total luminescence quenching is expected, because the excited electron in the thermally equilibrated excited state is no longer a barrier but rather on the transfer path. Further work with different metals and varying redox potentials is directed to substantiate or to disprove the conception concluded from our results. In addition, transient absorption spectroscopy will be tackled to provide conclusive evidence on the very fast energy transfer processes.

ASSOCIATED CONTENT

Supporting Information

Both 1D and 2D NMR spectroscopic data, EPR spectra of **7** and **8**-PF_6, molecular structure of **10**-PF_6 in the crystal, time-dependent and room- and low-temperature luminescence measurement data. Computational details: selected calculated and experimental metric parameters, Kohn−Sham frontier orbitals of $\mathbf{6a}^+$ and $\mathbf{10}^+$, spin density distribution of triplet states of $\mathbf{5a}^{2+}$, $\mathbf{6a}^+$ and $\mathbf{10}^+$, tables of additional results of TD-DFT calculations with the classical b3lyp functional, calculated UV−vis spectra, and crystallographic information files in CIF format. This material is available free of charge via the Internet at http://pubs.acs.org.

AUTHOR INFORMATION

Corresponding Authors

*E-mail: antje.neubauer@uni-rostock.de.
*E-mail: wolfram.seidel@uni-rostock.de.

Notes

The authors declare no competing financial interest.

ACKNOWLEDGMENTS

We thank Prof. A. Brückner (Leibniz Institute of Catalysis) for the EPR measurement. Financial support by the Deutsche Forschungsgemeinschaft (SE 890/3-1) and by the BMBF program "Spitzenforschung & Innovation in den Neuen Ländern" for the project "Light2Hydrogen" is gratefully acknowledged.

REFERENCES

(1) (a) Sauvage, J.-P.; Collin, J.-P.; Chambron, J.-C.; Guillerez, S.; Coudret, C.; Balzani, V.; Barigelletti, F.; De Cola, L.; Flamigni, L. *Chem. Rev.* **1994**, *94*, 993−1019. (b) Balzani, V.; Juris, A.; Venturi, M.; Campagna, S.; Serroni, S. *Chem. Rev.* **1996**, *96*, 759−833. (c) De Cola, L.; Belser, P. *Coord. Chem. Rev.* **1998**, *177*, 301−346. (d) Campagna, S.; Serroni, S.; Puntoriero, F.; Loiseau, F.; De Cola, L.; Kleverlaan, C.

J.; Becher, J.; Sorensen, A. P.; Hascoat, P.; Thorup, N. *Chem.—Eur. J.* **2002**, *8*, 4461−4469. (e) Ott, S.; Borgström, M.; Kritikos, M.; Lomoth, R.; Bergquist, J.; Akermark, B.; Hammarström, L.; Sun, L. *Inorg. Chem.* **2004**, *43*, 4683−4692. (f) Staniszewski, A.; Heuer, W. B.; Meyer, G. J. *Inorg. Chem.* **2008**, *47*, 7062−7064. (g) Laine, P. P.; Campagna, S.; Loiseau, F. *Coord. Chem. Rev.* **2008**, 2552−2571. (h) Walther, M. E.; Wenger, O. S. *ChemPhysChem* **2009**, *10*, 1203−1206. (i) Hammarström, L.; Johansson, O. *Coord. Chem. Rev.* **2010**, *254*, 2546−2559. (j) Manbeck, G. F.; Brewer, K. J. *Coord. Chem. Rev.* **2013**, *257*, 1660−1675. (k) Dietrich, J.; Thorenz, U.; Förster, C.; Heinze, K. *Inorg. Chem.* **2013**, *52*, 1248−1264. (l) Dietrich, J.; Leupoldt, A. W. v.; Grabolle, M.; Resch-Genger, U.; Heinze, K. *Eur. J. Inorg. Chem.* **2013**, 3009−3019.

(2) Grätzel, M. *Inorg. Chem.* **2005**, *44*, 6841−6851.

(3) (a) You, Y.; Park, S. Y. *Dalton Trans.* **2009**, 1267−1282. (b) Fantacci, S.; De, A. F. *Coord. Chem. Rev.* **2011**, *255*, 2704−2726. (c) You, Y.; Nam, W. *Chem. Soc. Rev.* **2012**, *41*, 7061−7084. (d) Happ, B.; Winter, A.; Hager, M. D.; Schubert, U. S. *Chem. Soc. Rev.* **2012**, *41*, 2222−2255.

(4) Ladouceur, S.; Zysman-Colman, E. *Eur. J. Inorg. Chem.* **2013**, 2985−3007.

(5) (a) Rau, S.; Schäfer, B.; Gleich, D.; Anders, E.; Rudolph, M.; Friedrich, M.; Görls, H.; Henry, W.; Vos, J. G. *Angew. Chem., Int. Ed.* **2006**, *45*, 6215−6218. (b) Fihri, A.; Artero, V.; Razavet, M.; Baffert, C.; Leibl, W.; Fontecave, M. *Angew. Chem., Int. Ed.* **2008**, *47*, 564−567.

(6) (a) Elvington, M.; Brown, J.; Arachchige, S. M.; Brewer, K. J. *J. Am. Chem. Soc.* **2007**, *129*, 10644−10645. (b) Nicewicz, D. A.; MacMillan, D. W. C. *Science* **2008**, *322*, 77−80. (c) Inagaki, A.; Akita, M. *Coord. Chem. Rev.* **2010**, *254*, 1220−1239. (d) Narayanam, J. M. R.; Stephenson, C. R. J. *Chem. Soc. Rev.* **2011**, *40*, 102−113. (e) Hollmann, D.; Gärtner, F.; Ludwig, R.; Barsch, E.; Junge, H.; Blug, M.; Hoch, S.; Beller, M.; Brückner, A. *Angew. Chem., Int. Ed.* **2011**, *50*, 10246−10250. (f) Gärtner, F.; Boddien, A.; Barsch, E.; Fumino, K.; Losse, S.; Junge, H.; Hollmann, D.; Brückner, A.; Ludwig, R.; Beller, M. *Chem.—Eur. J.* **2011**, *17*, 6425−6436. (g) Fukuzumi, S.; Kobayashi, T.; Suenobu, T. *Angew. Chem., Int. Ed.* **2011**, *50*, 728−731. (h) Tamaki, Y.; Koike, K.; Morimoto, T.; Yamazaki, Y.; Ishitani, O. *Inorg. Chem.* **2013**, *52*, 11902−11909.

(7) Bomben, P. G.; Robson, K. C. D.; Koivisto, B. D.; Berlinguette, C. P. *Coord. Chem. Rev.* **2012**, *256*, 1438−1450.

(8) (a) Lee, P.-K.; Law, W. H.-T.; Liu, H.-W.; Lo, K. K.-W. *Inorg. Chem.* **2011**, *50*, 8570−8579. (b) Moromizato, S.; Hisamatsu, Y.; Suzuki, T.; Matsuo, Y.; Abe, R.; Aoki, S. *Inorg. Chem.* **2012**, *51*, 12697−12706. (c) McConnell, A. J.; Song, H.; Barton, J. K. *Inorg. Chem.* **2013**, *52*, 10131−10136. (d) Leung, K.-H.; He, H.-Z.; Ma, V. P.-Y.; Chan, D. S.-H.; Leung, C.-H.; Ma, D.-L. *Chem. Commun.* **2013**, *49*, 771−773. (e) Tang, Y.; Yang, H.-R.; Sun, H.-B.; Liu, S.-J.; Wang, J.-X.; Zhao, Q.; Liu, X.-M.; Xu, W.-J.; Li, S.-B.; Huang, W. *Chem.—Eur. J.* **2013**, *19*, 1311−1319. (f) Zhang, R.; Ye, Z.; Song, B.; Dai, Z.; An, X.; Yuan, J. *Inorg. Chem.* **2013**, *52*, 10325−10331.

(9) Sun, J.; Zhong, F.; Yi, X.; Zhao, J. *Inorg. Chem.* **2013**, *52*, 6299−6310.

(10) Tschierlei, S.; Presselt, M.; Kuhnt, C.; Yartsev, A.; Pascher, T.; Sundström, V.; Karnahl, M.; Schwalbe, M.; Schäfer, B.; Rau, S.; Schmitt, M.; Dietzek, B.; Popp, J. *Chem.—Eur. J.* **2009**, *15*, 7678−7688.

(11) (a) Fox, G. A.; Bhattacharya, S.; Pierpont, C. G. *Inorg. Chem.* **1991**, *30*, 2895−2899. (b) Paw, W.; Eisenberg, R. *Inorg. Chem.* **1997**, *36*, 2287−2293.

(12) Paw, W.; Cummings, S. D.; Mansour, M. A.; Connick, W. B.; Geiger, D. K.; Eisenberg, R. *Coord. Chem. Rev.* **1998**, *171*, 125−150.

(13) Rabaca, S.; Duarte, M. C.; Santos, I. C.; Pereira, L. C. J.; Fourmigué, M.; Henriques, R. T.; Almeida, M. *Polyhedron* **2008**, *27*, 1999−2006.

(14) Chesneau, B.; Passelande, A.; Hudhomme, P. *Org. Lett.* **2009**, *11*, 649−652.

(15) Keniley, L. K., Jr.; Ray, L.; Kovnir, K.; Dellinger, L. A.; Hoyt, J. M.; Shatruk, M. *Inorg. Chem.* **2010**, *49*, 1307−1309.

(16) Keniley, L. K., Jr.; Dupont, N.; Ray, L.; Ding, J.; Kovnir, K.; Hoyt, J. M.; Hauser, A.; Shatruk, M. *Inorg. Chem.* **2013**, *52*, 8040−8052.

(17) Kirk, M. L.; McNaughton, R. L.; Helton, M. E. *Prog. Inorg. Chem.* **2004**, *52*, 111−212.

(18) Wang, K. *Prog. Inorg. Chem.* **2004**, *52*, 267−314.

(19) Nakamaru, K. *Bull. Chem. Soc. Jpn.* **1982**, *55*, 2697−2705.

(20) Morris, J. V.; Mahaney, M. A.; Huber, J. R. *J. Phys. Chem.* **1976**, *80*, 969−974.

(21) Gorelsky, S. I.; Lever, A. B. P. *J. Organomet. Chem.* **2001**, *635*, 187−196.

(22) (a) Vosko, S. H.; Wilk, L.; Nusair, M. *Can. J. Phys.* **1980**, *58*, 1200−1211. (b) Becke, A. D. *Phys. Rev. A* **1988**, *38*, 3098−3100. (c) Lee, C.; Yang, W.; Parr, R. G. *Phys. Rev. B* **1988**, *37*, 785−789. (d) Becke, A. D. *J. Chem. Phys.* **1993**, *98*, 5648−5652. (e) Bauschlicher, C. W.; Partridge, H. *Chem. Phys. Lett.* **1994**, *231*, 277−282.

(23) Yanai, T.; Tew, D. P.; Handy, N. C. *Chem. Phys. Lett.* **2004**, *393*, 51−57.

(24) (a) Ikura, H.; Tsuneda, T.; Yanai, T.; Hirao, K. *J. Chem. Phys.* **2001**, *115*, 3540. (b) Tawada, Y.; Tsuneda, T.; Yanagisawa, S.; Yanai, T.; Hirao, K. *J. Chem. Phys.* **2004**, *120*, 8425. (c) Chiba, M.; Tsuneda, T.; Hirao, K. *J. Chem. Phys.* **2006**, *124*, 144106.

(25) (a) Andrae, D.; Häußermann, U.; Dolg, M.; Stoll, H.; Preuß, H. *Theor. Chim. Acta* **1990**, *77*, 123−141. (b) Martin, J. M. L.; Sundermann, A. *J. Chem. Phys.* **2001**, *114*, 3408−3420.

(26) Gerber, R. E.; Hasbun, C.; Dubenko, L. G.; King, M. F.; Bierer, D. E. *Org. Synth.* **2000**, *77*, 186−197.

(27) (a) Trost, B. M.; Older, C. M. *Organometallics* **2002**, *21*, 2544−2546. (b) Rüba, E.; Simanko, W.; Mauthner, K.; Soldouzi, K. M.; Slugovc, C.; Mereiter, K.; Schmid, R.; Kirchner, K. *Organometallics* **1999**, *18*, 3843−3850.

(28) Sullivan, B. P.; Salmon, D. J.; Meyer, T. J. *Inorg. Chem.* **1978**, *17*, 3334−3341.

(29) Sprouse, S.; King, K. A.; Spellane, P. J.; Watts, R. J. *J. Am. Chem. Soc.* **1984**, *106*, 6647−6653.

(30) Bomfim, J. A. S.; Souza, F. P. d.; Filgueiras, C. A. L.; Sousa, A. G. d.; Gambardella, M. T. P. *Polyhedron* **2003**, *22*, 1567−1573.

(31) Newkome, G. R.; Theriot, K. J.; Fronczek, F. R.; Villar, B. *Organometallics* **1989**, *8*, 2513−2523.

(32) (a) Kutoglu, A. *Z. Anorg. Allg. Chem.* **1972**, *390*, 195−209. (b) Balz, H.; Köpf, H.; Pickardt, J. *J. Organomet. Chem.* **1991**, *417*, 397−406. (c) Hahn, F. E.; Seidel, W. W. *Angew. Chem., Int. Ed.* **1995**, *34*, 2700−2703. (d) Seidel, W. W.; Hahn, F. E.; Lügger, T. *Inorg. Chem.* **1998**, *37*, 6587−6596.

(33) Qin, J.; Hu, L.; Li, G.-N.; Wang, X.-S.; Xu, Y.; Zuo, J.-L.; You, X.-Z. *Organometallics* **2011**, *30*, 2173−2179.

(34) Dragonetti, C.; Falciola, L.; Mussini, P.; Righetto, S.; Roberto, D.; Ugo, R.; Valore, A.; Angelis, F. D.; Fantacci, S.; Sgamellotti, A.; Ramon, M.; Muccini, M. *Inorg. Chem.* **2007**, *46*, 8533−8547.

(35) (a) Zhao, Q.; Liu, S.; Shi, M.; Li, F.; Jing, H.; Yi, T.; Huang, C. *Organometallics* **2007**, *26*, 5922−5930. (b) Gärtner, F.; Cozzula, D.; Losse, S.; Boddien, A.; Anilkumar, G.; Junge, H.; Schulz, T.; Marquet, N.; Spannenberg, A.; Gladiali, S.; Beller, M. *Chem.—Eur. J.* **2011**, *17*, 6998−7006.

(36) (a) Velazquez, C. S.; Baumann, T. F.; Olmstead, M. M.; Hope, H.; Barrett, A. G. M.; Hoffman, B. M. *J. Am. Chem. Soc.* **1993**, *115*, 9997−10003. (b) Tian, Z.-Q.; Donahue, J. P.; Holm, R. H. *Inorg. Chem.* **1995**, *34*, 5567−5572. (c) Chesney, A.; Bryce, M. R.; Batsanov, A. S.; Howard, J. A. K. *Chem. Commun.* **1997**, 2293−2294. (d) Kaiwar, S. P.; Hsu, J. K.; Liable-Sands, L. M.; Rheingold, A. L.; Pilato, R. S. *Inorg. Chem.* **1997**, *36*, 4234−4240.

(37) (a) Beyer, B.; Ulbricht, C.; Escudero, D.; Friebe, C.; Winter, A.; Gonzalez, L.; Schubert, U. S. *Organometallics* **2009**, *28*, 5478−5488. (b) Ladouceur, S.; Fortin, D.; Zysman-Colman, E. *Inorg. Chem.* **2010**, *49*, 5625−5641. (c) Lo, K. K.-W.; Chan, J. S.-W.; Lui, L.-H.; Chung, C.-K. *Organometallics* **2004**, *23*, 3108−3116.

(38) Onozawa-Komatsuzaki, N.; Katoh, R.; Himeda, Y.; Sugihara, H.; Arakawa, H.; Kasuga, K. *Bull. Chem. Soc. Jpn.* **2003**, *76*, 977−984.

(39) (a) Kaiwar, S. P.; Vodacek, A.; Blough, N. V.; Pilato, R. S. *J. Am. Chem. Soc.* **1997**, *119*, 9211−9214. (b) Kaiwar, S. P.; Vodacek, A.; Blough, N. V.; Pilato, R. S. *J. Am. Chem. Soc.* **1997**, *119*, 3311−3316.
(40) Cummings, S. D.; Eisenberg, R. *J. Am. Chem. Soc.* **1996**, *118*, 1949−1960.
(41) Juris, A.; Balzani, V.; Barigelletti, F.; Campagna, S.; Belser, P.; von Zelewsky, A. *Coord. Chem. Rev.* **1988**, *84*, 85−277.
(42) (a) Glazer, E. C.; Magde, D.; Tor, Y. *J. Am. Chem. Soc.* **2007**, *129*, 8544−8551. (b) Baron, A.; Herrero, C.; Quaranta, A.; Charlot, M.-F.; Leibl, W.; Vauzeilles, B.; Aukauloo, A. *Chem. Commun.* **2011**, *47*, 11011−11013. (c) Hirahara, M.; Masaoka, S.; Sakai, K. *Dalton Trans.* **2011**, *40*, 3967−3978.
(43) Bokarev, S. I.; Hollmann, D.; Pazidis, A.; Neubauer, A.; Radnik, J.; Kühn, O.; Lochbrunner, S.; Junge, H.; Beller, M.; Brückner, A. *Phys. Chem. Chem. Phys.* **2014**, *16*, 4789−4796.
(44) Neubauer, A.; Grell, G.; Friedrich, A.; Bokarev, S. I.; Schwarzbach, P.; Gärtner, F.; Surkus, A.-E.; Junge, H.; Beller, M.; Kühn, O.; Lochbrunner, S. *J. Phys. Chem. Lett.* **2014**, *5*, 1355−1360.
(45) (a) Zeng, X.; Tavasli, M.; Perepichka, I. F.; Batsanov, A. S.; Bryce, M. R.; Chiang, C.-J.; Rothe, C.; Monkman, A. P. *Chem.—Eur. J.* **2008**, *14*, 933−943. (b) Costa, R. D.; Orti, E.; Bolink, H. J.; Graber, S.; Schaffner, S.; Neuburger, M.; Housecroft, C. E.; Constable, E. C. *Adv. Funct. Mater.* **2009**, *19*, 3456−3463. (c) Ma, L.; Guo, H.; Li, Q.; Guo, S.; Zhao, J. *Dalton Trans.* **2012**, *41*, 10680−10689. (d) Alam, P.; Laskar, I. R.; Climent, C.; Casanova, D.; Alemany, P.; Karanam, M.; Choudhury, A. R.; Raymond, B. J. *Polyhedron* **2013**, *53*, 286−294.
(46) (a) Bokarev, S. I.; Bokareva, O. S.; Kühn, O. *J. Chem. Phys.* **2012**, *136*, 214305. (b) Edkins, R. M.; Fucke, K.; Peach, M. J. G.; Crawford, A. G.; Marder, T. B.; Beeby, A. *Inorg. Chem.* **2013**, *52*, 9842−9860.
(47) (a) Alary, F.; Heully, J.-L.; Bijeire, L.; Vicendo, P. *Inorg. Chem.* **2007**, *46*, 3154−3165. (b) Yin, J.-F.; Bhattacharya, D.; Thanasekaran, P.; Hsu, C.-P.; Tseng, T.-W.; Lu, K.-L. *Inorg. Chim. Acta* **2009**, *362*, 5064−5072. (c) Ji, S.; Wu, W.; Wu, W.; Song, P.; Han, K.; Wang, Z.; Liu, S.; Guo, H.; Zhao, J. *J. Mater. Chem.* **2010**, *20*, 1953−1963.
(48) (a) Inagaki, A.; Edure, S.; Yatsuda, S.; Akita, M. *Chem. Commun.* **2005**, 5468−5470. (b) Inagaki, A.; Yatsuda, S.; Edure, S.; Suzuki, A.; Takahashi, T.; Akita, M. *Inorg. Chem.* **2007**, *46*, 2432−2445.
(49) (a) Duan, H.-S.; Chou, P.-T.; Hsu, C.-C.; Hung, J.-Y.; Chi, Y. *Inorg. Chem.* **2009**, *48*, 6501−6508. (b) Hedley, G. J.; Ruseckas, A.; Samuel, I. D. W. *Chem. Phys. Lett.* **2008**, *450*, 292−296.
(50) Sun, Q.; Mosquera-Vazquez, S.; Daku, L. M. L.; Guenee, L.; Goodwin, H. A.; Vauthey, E.; Hauser, A. *J. Am. Chem. Soc.* **2013**, *135*, 13660−13663.